1 **Evidence for dissolved organic matter as the primary source and sink of**

2 **photochemically produced hydroxyl radical in arctic surface waters**

3

4

5 Sarah E. Page[1], J. Robert Logan[1], Rose M. Cory[2]*, Kristopher McNeill[1]*

6

7 [1] Institute of Biogeochemistry and Pollutant Dynamics, Swiss Federal Institute of

8 Technology (ETH), Zurich, Switzerland;

9 [2] Department of Earth and Environmental Sciences, University of Michigan, Ann Arbor,

10 Michigan, USA.

11

12 * Corresponding authors

13   **Environmental Impact Statement**

14   Hydroxyl radical (•OH) is a reactive oxidant that has been implicated in carbon cycling

15   and fate of recalcitrant pollutants in aquatic ecosystems. Uncertainty about the sources

16   and sinks of •OH and their relative magnitudes in natural waters has hindered efforts to

17   understand these processes. To address these knowledge gaps, we characterized the

18   formation and reaction of photochemically produced •OH across a range of small streams,

19   large rivers, and lakes in the Arctic. Rates of photochemical •OH formation from

20   dissolved organic matter (DOM) in arctic surface waters were higher than expected given

21   the low levels of nitrate and relatively low levels of iron, suggesting that the DOM in

22   these waters may be better at generating •OH than has been previously characterized. We

23   concluded that DOM was the primary source and sink for •OH in these surface waters.

24

25   **TOC**
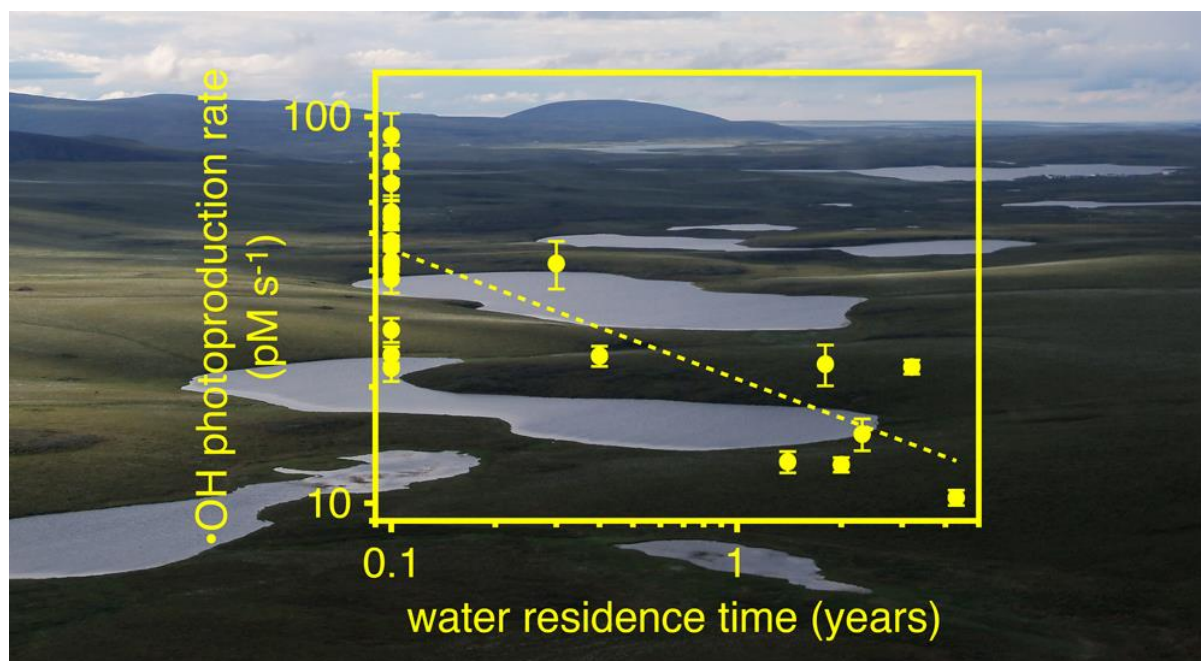
27   **Graphical Abstract Text**

28   Photochemical hydroxyl radical formation decreases with increasing water residence time

29   in a system of lakes connected by streams in the Arctic.

30 **Abstract**

31   Hydroxyl radical (•OH) is an indiscriminate oxidant that reacts at near–diffusion–

32 controlled rates with organic carbon. Thus, while •OH is expected to be an important

33 oxidant of dissolved organic matter (DOM) and other recalcitrant compounds, the role of

34 •OH in the oxidation of these compounds in aquatic ecosystems is not well known due to

35 the poorly constrained sources and sinks of •OH especially in pristine (unpolluted) natural

36 waters. We measured the rates of •OH formation and quenching across a range of surface

37 waters in the Arctic varying in concentrations of expected sources and sinks of •OH.

38 Photochemical formation of •OH was observed in all waters tested, with rates of

39 formation ranging from 2.6 ± 0.6 to $900 \pm 100 \times 10^{-12}$ M s^{-1}. Steady–state concentrations

40 ranged from 2 ± 1 to $290 \pm 60 \times 10^{-17}$ M, and overlapped with previously reported values in

41 surface waters. While iron–mediated photo–Fenton reactions likely contributed to the

42 observed •OH production, several lines of evidence suggest that DOM was the primary

43 source and sink of photochemically produced •OH in pristine arctic surface waters. DOM

44 from first–order or headwaters streams was more efficient in producing •OH than what

45 has previously been reported for DOM, and •OH formation decreased with increasing

46 residence time of DOM in sunlit surface waters. Despite the ubiquitous formation of •OH

47 in arctic surface waters observed in this study, photochemical •OH formation was

48 estimated to contribute ≤ 4 % to the observed photo–oxidation of DOM; however, key

49 uncertainties in this estimate must be addressed before ruling out the role of •OH in the

50 oxidation of DOM in these waters.

51

52   **Introduction**

53   Hydroxyl radical (•OH) is a potent oxidant of organic compounds in sunlit surface

54   waters, but uncertainty on the specific sources, sinks, and reactions of •OH with aquatic

55   constituents have limited efforts to quantify the role of •OH in aquatic C cycling. The role

56   of •OH in the oxidation of dissolved organic matter (DOM), the largest C pool in aquatic

57   ecosystems, depends on the magnitude of •OH production, which in turn is a function of

58   the sources and formation pathways of •OH. For example, under conditions conducive to

59   photo–Fenton processes, e.g. reaction of ferrous iron with hydrogen peroxide, •OH was

60   suggested to be an important oxidant of DOM to CO_2.[1-4] In contrast, when photochemical

61   reactions of DOM, nitrate, or nitrite were the predominant sources of •OH, rates of •OH

62   formation were concluded to be too low for •OH to account for the observed

63   mineralization of DOM.[5,6] However, we currently know too little about how the sources

64   and magnitude of photochemical •OH production (photo–Fenton vs. DOM or "other")

65   vary across aquatic ecosystems covering gradients in pH, iron, DOM concentration, and

66   DOM chemical composition to understand the importance of •OH in C cycling.

67   The photochemical sources of •OH in natural waters are nitrite,[7-9] nitrate,[8,10-13]

68   photo–Fenton reactions,[2,14] and DOM.[15-18] In waters receiving agricultural or urban run–

69   off, nitrate and nitrite are important sources of •OH formation. Iron–mediated photo–

70   Fenton sources of •OH are important in iron–rich waters, such as streams or ponds

71   polluted by acid–mine drainage. Photo–Fenton reactions may also contribute to •OH

72   formation in pristine low–iron waters. Vermilyea and Voelker estimated that ~ 80 nM of

73   iron was adequate to initiate photo–Fenton production of •OH in freshwaters and

74   suggested that even at these low iron concentrations photo–Fenton formation of •OH may

75   be comparable to surface waters containing up to 100 μM nitrate.[4] However, it is not

76   possible to predict the role of iron in •OH formation based only on iron concentrations

77   because •OH production does not necessarily increase linearly with added iron.[19] Inter–

78   related factors including pH, iron redox state and speciation, as well as sources and sinks

79   of the key intermediates, all contribute to the rate of •OH production from photo–Fenton

80   reactions.

81   Nonetheless, in polluted waters where concentrations of nitrate, nitrite, and iron

82   are high, these constituents are well–characterized sources of •OH. In contrast, many

83   pristine waters have low concentrations of these constituents and are instead high in

84   DOM.[20-22] Due to the chemical heterogeneity of DOM, the contribution of DOM to •OH

85   formation in natural waters has often been inferred "by difference", whereby the yields of

86   •OH from better–characterized sources (e.g. nitrate, nitrite, iron) are taken in account

87   based on their concentration and the remaining •OH is attributed to DOM.[6,23,24] For

88   example, using this approach, Mopper and Zhou found that nitrate, nitrite, and hydrogen

89   peroxide, an indicator of photo–Fenton sources, accounted for less than 50% of the

90   observed •OH.[15,16] To further support the role of DOM in the remaining > 50% of •OH

91   formed, Mopper and Zhou reported positive relationships between •OH production and

92   measures of the chromophoric and fluorescent fractions of DOM (i.e. CDOM and FDOM,

93   respectively).[15,16] Vaughan and Blough also concluded that DOM could account for at

94   least 50% of photochemical •OH in surface waters. In their study, they added catalase to

95   minimize the photo–Fenton source of •OH from trace metals present in well characterized

96   isolate of aquatic DOM.[17]

97   While studies have demonstrated that DOM plays a role in the photochemical

98   formation of •OH in surface waters, few studies have investigated patterns of •OH

99   formation across pristine waters where DOM is likely to be relatively more important

100   source of •OH compared to polluted waters with elevated levels of nitrate, nitrite and

101   iron. A notable exception is the recent work of Timko, et al., which examined the

102   production of •OH along an estuarine gradient in the Florida Everglades.[25] Of the studies

103   that have characterized •OH formation from isolated DOM in the laboratory, evidence has

104   suggested that the light–exposure history and chemical composition of DOM may

105   influence its capacity to produce •OH. For example, •OH production has been shown to

106   vary between sources of DOM differing in chemical composition[18,19] and has been

107   reported to decrease with increasing exposure of DOM to light.[26] These findings are

108   consistent with studies showing higher •OH production upon exposure of photo–protected

109   groundwater or bottom waters to sunlight, in comparison to •OH formation from surface

110   waters (accounting for differences in DOM concentration).[6,15] The degradation of

111   chromophoric DOM during exposure to light (photobleaching) would be expected to alter

112   •OH formation because it is the light–absorbing aromatic fraction of DOM that is

113   responsible for production of reactive oxygen species, including •OH.[27] Thus, the current

114   understanding is that in addition to iron, DOM is a source of •OH in pristine waters, and

115   its capacity to form •OH may vary with its light exposure history, e.g. residence time in

116   sunlit surface waters.

117   Although there is uncertainty on the relative importance of iron or DOM as

118   sources of •OH in pristine aquatic ecosystems, the fate of •OH once formed may be

119   constrained if the concentration of DOM and major anions are known. Hydroxyl radical

120   reacts at near–diffusion–controlled rates with many organic and inorganic compounds.[28]

121   In seawater or other high ionic strength freshwaters, the majority of the •OH formed

122   reacts with anions to form radical species of lower energy and higher reaction

123   selectivity,[15] with less •OH available to oxidize DOM. In contrast, in oligotrophic or low

124   ionic strength freshwaters, DOM is expected to be the major sink for •OH for DOM

125   concentrations ≥ 0.5 mg C/L.[5,13] However, few studies have measured the rate constant of

126   •OH quenching in freshwaters exhibiting gradients in DOM and major anions. While

127 studies have verified that DOM is the main sink for •OH in low conductivity waters

128 prepared using isolates or extracts of DOM in DI water, a lack of field measurements in

129 freshwaters covering gradients in DOM composition means there is little information to

130 guide expectations on how the quenching of •OH by DOM may vary with DOM

131 composition.

132 To address these knowledge gaps, we conducted a field survey of sources and

133 sinks of •OH in arctic surface waters near the Arctic Long–Term Ecological Research

134 (LTER) site at Toolik Lake, Alaska, USA (68° 38' N, 149° 36' W) covering gradients in

135 water chemistry that likely enhance or minimize •OH production (e.g. pH and

136 concentrations of dissolved constituents involved in the production and quenching of

137 •OH). For example, we sampled small, acidic headwater streams rich in DOM and iron,

138 as well as the circumneutral lakes receiving water from these streams. We also compared

139 •OH production and quenching along longitudinal transects on two large rivers, the

140 Kuparuk, whose headwaters are isolated from glaciers in the Brooks Range, and the

141 Sagavanirktok, whose headwaters arise in the mountains and whose water is impacted

142 strongly by carbonate-rich rocks and glacial flour. These two rivers thus have contrasting

143 characteristics of low dissolved organic carbon (DOC) and high dissolved inorganic

144 carbon (DIC) in the Sagavanirktok, and high DOC and low DIC in the Kuparuk and they

145 also represent the two major types of rivers draining into the Arctic Ocean.[29,30]

146 Because our goal was to test for the influence of DOM on photochemical

147 production and quenching of •OH, we sampled a configuration of lakes and streams that

148 have strong downstream gradients in DOM composition. For example, we compared

149 water from two branches of the Inlet Series stream differing in lake–stream

150 configurations. One stream branch contains a chain of nine lakes while the other stream

151 branch serves as a "control" because it has only one lake near its base fed by a large

152   network of headwater streams. Because the contrasting branches are adjacent and thus

153   drain the same soils (and thus have similar chemistry at their headwaters), the major

154   difference between the branches is the longer residence time of the water in the branch

155   with lakes compared to the lake-less branch.[20] The stream connecting lakes functions

156   differently than a lake-less stream due to the cumulative effects of moving materials from

157   lake to lake and the associated increased residence times in lakes compared to

158   streams,[20,31] consistent with the correlation between DOM composition and water

159   residence time in these surface waters.[32] Together, previous studies of the Inlet Series and

160   nearby streams and lakes has suggested that water residence time is an important control

161   on DOM composition due to increased opportunities for soil-derived DOM to be

162   degraded by bacteria and sunlight in surface waters.[20,31,32] Similarly, DOM processing at

163   the headwaters of a river may differ compared to processing at the river mouth due to

164   downstream increases in light exposure.[33] Thus, we measured •OH production and

165   quenching from different configurations of lakes and streams and from a longitudinal

166   transect of a large river to infer how the processing of DOM with increased water

167   residence time may influence the photochemical production and fate of •OH.

168   Finally, given that •OH has been implicated in the photochemical oxidation of

169   DOM to CO_2, we were also motivated to investigate •OH sources and sinks in arctic

170   surface waters because there is increasing consensus that, on a landscape level,

171   photochemical oxidation of DOM is important for the fate of terrestrially derived DOM

172   flushed from soils to sunlit surface waters in the Arctic.[32,34-36] Strong climate change in

173   the Arctic is leading to permafrost thaw,[37] which can cause melting of ground ice and

174   destabilization leading to hillslope failures (i.e. thermokarst failures).[38] An anticipated

175   consequence of permafrost thaw and thermokarst failure is the increased flow of DOM

176   from soils to sunlit surface waters where this previously frozen C may be oxidized and

177   returned to the atmosphere as CO_2 by photochemical reactions involving •OH, among

178   other processes.

179

180   **Materials and Methods**

181   *General considerations*

182   Site Description

183   Water samples were collected from 65 surface waters near the Arctic Long−Term

184   Ecological Research (LTER) site at Toolik Lake, Alaska, USA (68° 38' N, 149° 36' W;

185   elevation 720 m) during snowmelt and the ice−free season (May−August) 2012.[20,32] The

186   area around Toolik Field Station is characterized by continuous permafrost and nearly 24

187   hours of daylight during the summer growing season (May−August). In contrast, in the

188   winter months (September−April) with little to no daylight, the streams and lakes are

189   frozen and snow−covered. Ice−out and snowmelt generally occur in May or June.

190   Snowmelt corresponds with the peak discharge in streams and rivers,[39] with higher DOM

191   concentrations[39] and shifts in DOM composition[39,40] compared to the much lower flow

192   conditions thereafter through the summer.

193   Tussock tundra is the dominant vegetation, and areas of wet sedge tundra, drier

194   heath tundra on ridge tops and other well−drained sites with river−bottom willow

195   communities are found in the Toolik Lake watershed (http://ecosystems.mbl.edu/ARC/).

196   Surface waters near Toolik Lake are ultra−oligotrophic[20] and exhibit a large range in

197   concentrations of DOM and dissolved iron.[32,34,41,42]

198   We collected water at different spatial and temporal scales over the summer. For

199   example, samples were collected ca. biweekly to monthly at Imnavait Creek, a first−order

200   stream characterized by low pH (5−6), low conductivity (avg. 14 µS cm^{-1}), and high DOC

201   (avg. 1300 µM C),[43] and from the Kuparuk River near the field station where the river is

202   a 4th order stream characterized by near–neutral pH (> 7), medium conductivity (avg. 100

203   µS cm^{−1}), and medium DOC (avg. 420 µM C). Approximately monthly samples were also

204   collected from the Sagavanirktok River, characterized by alkaline pH (~8), high

205   conductivity (avg. 230 µS cm^{−1}), and low DOC (avg. 110 µM C), as well as the Toolik

206   Inlet stream, a second–order stream characterized by near–neutral pH (>7), medium

207   conductivity (avg. 70 µS cm^{−1}), and medium DOC (avg. 600 µM C).

208   In addition, we sampled hydrologically connected streams and lakes at two spatial

209   scales in August 2012 to test the role of residence time in sunlit surface waters on the

210   photochemical production of •OH. First, on a spatial scale of ~ 18 km, we sampled the

211   Inlet Series stream of Toolik Lake Catchment from its headwaters to Tooilk Lake. The

212   Inlet Series stream consists of two major branches: (1) the western branch passing

213   through a series of eight lakes before reaching Toolik Lake (2) the eastern branch that

214   flows only through the tundra for its entire length until it reaches the last lake upstream of

215   Toolik Lake.[20] The Inlet Series streams range in order from 1–3, and the water chemistry

216   is characterized by near–neutral pH, low-medium conductivity (avg. 50 µS cm^{−1}), and

217   medium DOC (avg. 600 µM C).

218   Secondly, on a spatial scale of ~ 350 km we collected water from 10 sites

219   spanning the Kuparuk River from its headwaters in the Brooks Range to the mouth at the

220   Arctic Ocean. The Kuparuk River water chemistry varies from the headwaters to the coast

221   with pH ~7, conductivity ~ 100 µS cm^{−1}, and ~ 400 µM C in the 1st–3rd order upstream

222   sections to pH ~8, conductivity ~ 100 µS cm^{−1}, and ~ 300 µM C, downstream where the

223   river is ≥ 4th order.

224   Lastly, we also sampled thermokarst soil waters and thermokarst–impacted surface

225   waters. Thermokarst–impacted streams and lakes receive inputs of permafrost carbon and

226   minerals as the result of a thawing–induced landscape failure and are characterized by

227   high conductivity (~ 700 µS cm^{-1}), high DOC (~ 2100 µM C), and high alkalinity (~ 1700

228   µeq L^{-1}).[34]

229   Chemicals

230   All chemicals were used as received, unless otherwise noted. Suwannee River

231   Fulvic Acid (SRFA; 1S101F) was obtained from the International Humic Substances

232   Society (IHSS). Terephthalic acid (98%) and 2–hydroxyterephthalic acid (97%) were

233   obtained from Aldrich. Sodium terephthalate (TPA) was prepared as previously

234   described.[44] Ferrous ammonium sulfate (ACS grade), 3–(2–pyridyl)–5,6–diphenyl–1,2,4–

235   triazine–p,p'–disulfonic acid disodium salt hydrate (ferrozine; ≥98%), 4–(2–

236   hydroxyethyl)piperazine–1–ethanesulfonic acid (HEPES; ≥99.5%), hydroxylamine

237   hydrochloride (≥99%), potassium phosphate monobasic (reagent grade), sodium

238   phosphate dibasic anhydrous (reagent grade), mercuric chloride (>99%), sodium

239   hydroxide (1.0 N solution, certified), and hydrochloric acid (trace metal grade) were

240   obtained from Fisher Scientific. Formic acid (AnalaR Normapure, 99–100%) was

241   obtained from VWR. Pyridine (99.9%), *p*–nitroanisole (97%), and methanol (Chromasolv

242   for HPLC) was obtained from Sigma–Alrich. Water for stock solutions was obtained from

243   a Barnstead E–Pure and B–Pure deionization system or Millipore Simplicity UV System.

244

245   *Sample collection*

246   Under high flow conditions (e.g. early season), water samples were collected as

247   grab samples in triple-rinsed HDPE bottles from the bank of streams. Under low flow

248   conditions during July- August, water samples were collected close to the center of the

249   shallow streams and rivers (mean depth of 0.5 m). Most collection of lake surface waters

250   was taken as grab samples from the bank of the lake outlet stream, because the water

251   flowing to the lake outlet is an integrated sample of epilimnetic water.[20] Exceptions to the

252   lake outlet grab samples included surface water from Toolik Lake in May when the lake

253   was ice−covered; on this date water was collected a depth of 3m (ice thickness ~ 1 m) by

254   pumping water up to the surface using a peristaltic pump. All water samples were filtered

255   at Toolik Lake Field Station using pre−combusted GF/F filters (nominal 0.7 μm;

256   Whatman), unless otherwise noted. All samples were stored at 4 °C until analysis which

257   ranged from hours (for UV−vis/fluorescence characterization) to months for •OH, DOC,

258   or total iron analysis.

259

260   *Sample characterization*

261   Temperature, pH, and conductivity were measured *in situ* in the field using Orion

262   or WTW pH and conductivity meters. Alkalinity was measured using potentiometric

263   titrations and analyzed with the Gran method. Dissolved organic carbon (DOC) was

264   measured from GF/F (nominal 0.7 μm; Whatman) filtered water from filtered water

265   samples preserved with 6 N HCl using a Shimadzu TOC−V analyzer.[20]

266   Samples for UV−visible absorbance and fluorescence spectra were analyzed in the

267   field from filtered water using an Aqualog Fluorometer (Horiba Scientific). Fluorescence

268   spectra were collected as excitation−emission matrices (EEMs) following procedures in

269   Cory et al. 2010.[45]

270   Aliquots of water filtered in the field were acidified to pH ~2 with 6 N trace metal

271   grade HCl prior to analysis of total and ferrous iron via the ferrozine method.[46] Samples

272   for total iron analysis via ICP were filtered in the field using Whatman nylon 0.45 μm

273   filters followed by acidification to pH ~ 2 with 6 N trace metal grade HCl.

274

275   *Hydroxyl radical detection*

276   Hydroxyl radical production was measured using terephthalate (TPA) as a probe.

277   TPA has been used to detect photochemical •OH production from natural waters[47] and

278   from natural organic matter isolate solutions.[18,44,48-56] Briefly, TPA was added to natural

279   water samples placed in borosilicate test tubes and exposed to UV light. Simulated UV

280   light is required to measure •OH formation because the hTPA is not stable when exposed

281   to the higher energy wavelengths in the UVB portion of sunlight.[44] Two different

282   procedures were used for the photolysis and measurements, depending on the location of

283   the analysis (Toolik Field Station or ETH Zurich; see Table S1 in the supporting

284   information for sample information and measurement location).

285   At the field station, photolysis experiments were conducted using 6×40–W

286   BL350 fluorescent blacklight tubes fixed to the top of the photolysis chamber,[34] with

287   samples placed horizontally on a rotating plate, and subsamples taken for analysis over

288   the course of two hours. The fluorescence of the subsamples was measured ($\lambda_{ex} = 310$ nm,

289    $\lambda_{em} = 425$ nm). Standard addition of 0, 40, and 80 nM hTPA was used to calibrate the

290   hTPA response for each sample. At ETH Zurich, photolysis experiments were conducted

291   using a Rayonet reactor with 2×365 nm bulbs located on the outside walls of the reactor

292   and a rotating merry–go–round sample holder at the center of the reactor, with

293   subsamples taken over the course of 1 hour and analyzed via UPLC, using a method

294   published previously.[18,44,57] The intensity of the Rayonet light source used in this study

295   has been shown to be slightly more intense but overall similar to sunlight,[58] comparable

296   with light sources used in other studies. Because the rate of •OH formation is dependent

297   on the light source and intensity, and a subset of samples was analyzed using both light

298   sources (at the field station and in the laboratory) to determine that values obtained for

299   the samples exposed to the blacklight fluorescent bulb at the field station were on average

300   60 ± 10 % lower than values obtained for samples exposed to the Rayonet in the

301   laboratory, due to the lower intensity of the fluorescent bulbs at the field station. All data

302   measured at the field station using the blacklight fluorescence bulbs were corrected for

303   this factor. Given the lower sensitivity of the fluorescence–based method used to detect

304   •OH at the field station compared to the combined LC–fluorescence method used in the

305   laboratory, as well as the lower overall •OH production due to the different light source,

306   we were unable to quantify •OH quenching rates for samples analyzed at the field station.

307   The limit of detection for the fluorescence–based method was ~ 4 nM, while the limit of

308   detection for the combined LC–fluorescence method was < 1 nM. The standard deviation

309   of the hTPA fluorescence response was an average of ±7%, providing evidence for

310   minimal matrix interference effects in the measurements.

311   Additionally, the rates of hTPA formation were corrected for internal light

312   screening at the major excitation wavelength (λ=340 nm for the field method; λ=365 nm

313   for the Rayonet in the laboratory), using the following equation (1)

314    $$S_\lambda = \frac{1-e^{a_\lambda l}}{a_\lambda l} \tag{1}$$

315   where a_λ is the Naperian absorption coefficient in cm^{-1}, and l is the photolysis path length

316   in cm.

317   Two concentrations of the TPA probe compound were added to splits of each

318   sample to quantify •OH formation and quenching. A concentration of 850 μM TPA was

319   used to quantify the rate of formation of •OH (equation 2), because this concentration was

320   calculated to be sufficient to quantitatively react with the •OH formed during photolysis.

321   This calculation assumes a yield of hTPA formation of 0.35 for each reaction of TPA

322   with •OH.[44] There is currently no method to explicitly account for any sample–to–sample

323   variability in hTPA yield. While there is evidence that this yield does not depend on

324   DOM composition, pH, or DO concentrations,[59-61] the effect of iron concentration or

325   conductivity on the yield of hTPA has not been studied in natural waters. The error in the

326   rate of formation was calculated as the regression uncertainty of the slope of hTPA

327   concentration versus photolysis time (±10% on average). A second split of each sample

328   was spiked with 11 μM TPA to quantify the rate constant of quenching of •OH,

329   subsequently calculated using the concurrently quantified rate of formation (equation 3).

330   A concentration of 11 μM TPA was chosen because it had previously been demonstrated

331   to provide a balance between sufficient hTPA formation and minimal perturbation of the

332   steady–state •OH concentration.[18,44] The error in the rate constant of quenching (an

333   average of ±14%) was determined using the standard deviation of the slope of hTPA

334   concentration versus photolysis time and the error in the rate of formation. The steady–

335   state concentration of •OH was calculated using the rate of formation and the rate of

336   quenching of •OH (equation 4), with the error propagated from the rates of formation and

337   quenching (±16% on average).

338    $$k_{form,•OH} = \frac{[hTPA]/time}{0.35} \tag{2}$$

339    $$k_{quench,•OH} = \left[\frac{0.35 k_{form,•OH}}{[hTPA]/time} - 1\right] \times (k_{rxn,TPA}[TPA]) \tag{3}$$

340    $$[•OH]_{ss} = \frac{k_{form,•OH}}{k_{quench,•OH}} \tag{4}$$

341

342   *Calculation of hydroxyl radical production quantum yield*

343   The apparent quantum yield ($\phi_{•OH}$) of •OH production was calculated to normalize

344   the observed rate of •OH production to the rate of light absorption of each water sample,

345   such that highly colored waters could be compared to waters with lower absorbance. For

346   calculations of apparent quantum yield of •OH production ($\phi_{•OH}$), a *p*–

347   nitroanisole/pyridine (PNA–pyr) actinometer was used to quantify the irradiance in the

348   Rayonet reactor, a polychromatic UVA light source (340–410 nm) using a method

349   previously described[62] to calculate the apparent $\phi_{•OH}$ for each sample using equation 5.

350   All absorbance values for water samples, actinometers, and Suwanee River Fulvic Acid,

351   were low (below 0.15 at 365 nm), and the actinometer reaction was measured to the

352   completion of one half–life. The error in these values was quantified as the standard

353   deviation of rates of •OH production and PNA degradation, which was on average ±8%.

354     $$\phi_{\bullet OH} = \frac{k_{form,\bullet OH}}{k_{PNA}} \times \frac{k_{abs,PNA}}{k_{abs,\bullet OH}} \times \phi_{PNA} \tag{5}$$

355   In this equation, the $\phi_{\bullet OH}$ is the ratio of the rates of •OH production from the natural water

356   samples ($k_{form,\bullet OH}$) and the PNA degradation observed (k_{PNA}), multiplied by the ratio of

357   the light absorption from 340–410 nm of the PNA ($k_{abs,PNA}$) and the water sample

358   ($k_{abs,\bullet OH}$), multiplied by the apparent quantum yield of the PNA/pyr actinometer (ϕ_{PNA}).

359   To confidently compare apparent quantum yields for •OH quantified in this study

360   to previously published values, we measured the apparent quantum yield for •OH

361   production from a well–characterized reference DOM sample from the International

362   Humic Substance Society, Suwanee River Fulvic Acid (SRFA). The rate of •OH

363   production for SRFA was determined to be $71\pm4 \times 10^{-12}$ M s^{-1} for a solution with 12 mg C

364   L^{-1} at 365 nm, in agreement with previously measured values ($13–60\times10^{-12}$ M s^{-1})

365   obtained under similar irradiation conditions.[3,17] The $\phi_{\bullet OH}$ value for SRFA was found to

366   be $2.7\pm0.1 \times 10^{-5}$, in good agreement with previous findings at 360 nm ($\sim 2.4 \times 10^{-5}$).[17]

367

368   *Correlation of water quality parameters with hydroxyl radical formation and quenching*

369   To evaluate the variation in •OH among the data, •OH formation and quenching

370   rates were compared with > 20 measures of DOM quantity and quality or water

371   chemistry: a_{CDOM} (integrated absorbance, a_{300}, a_{305}, a_{313}, a_{320}, a_{340}, a_{365}, a_{380}, a_{395}, a_{412},

372   slope ratio), FDOM (integrated fluorescence, peak A, peak C, peak T, fluorescence

373   index), total iron, ferrous iron, ferric iron, DOC, alkalinity, pH, conductivity, and water

374   temperature. Using linear regression analysis, significant correlations were reported based

375   on a slope significantly different than zero (95% CI). Because [•OH]$_{ss}$ is the ratio of the

376   rates of •OH formation and quenching, the correlations were a combination of the

377   relationships observed individually for the formation and quenching and thus were not

378   reported here.

379   **Results**

380   *Water chemistry overview*

381   Imnavait Creek had the lowest conductivity and alkalinity, high DOC, and highest

382   dissolved iron concentrations (980–2200 μM C and 4–11 μM Fe, see Table 1) as expected

383   given that this stream drained the water–logged organic mat of the active soil layer.[43]

384   Imnavait Creek was poorly buffered and, due to the abundance of organic acids flushed

385   from soils, generally had low pH (4.8–6.6). Low pH likely slowed oxidation of the

386   continuous flux of reduced iron from the anoxic soils, leading to the observed high

387   ferrous iron concentrations of 2–6 μM in comparison to other surface waters (Table 1).

388   Other streams and lakes (Inlet Series, Toolik Lake, Kuparuk River, Sagavanirktok River),

389   exhibited a wider range of conductivity, pH, and alkalinity, but were generally lower in

390   DOC and Fe and higher in conductivity and alkalinity compared to waters from Imnavait

391   Creek (Table 1). Waters from thermokarst soils had the highest conductivity, DOC, and

392   alkalinity due to the weathering of carbonate–rich minerals and organic matter in

393   permafrost soils.

394

395

396   **Table 1.** Water chemistry measurements for all samples.[a]

Variable	Surface Waters[b]	Imnavait Creek	Thermokarst Soil Waters
Sample number =	102	6	8
pH	6.98 ± 0.06	5.2 ± 0.5 [c]	7.4 ± 0.04
Conductivity ($\mu S\ cm^{-1}$)	114 ± 7 [d]	14 ± 3 [d]	700 ± 200 [d]
Alkalinity ($\mu eq\ L^{-1}$)	760 ± 60	29 ± 5 [c]	2000 ± 1000
DOC ($\mu mol\ L^{-1}$)	440 ± 20 [d]	1300 ± 200 [d]	2100 ± 600 [d]
Integrated absorbance (m^{-1})	820 ± 70 [d]	3500 ± 1400 [d]	2000 ± 300 [d]
a_{320} (m^{-1})	12 ± 1 [d]	52 ± 6 [d]	28 ± 3 [d]
Integrated fluorescence	5200 ± 400 [d]	21000 ± 2000 [d]	27000 ± 3000 [d]
Peak A	0.87 ± 0.06 [c]	3.4 ± 0.3	3.6 ± 0.4
Peak C	0.39 ± 0.03 [c]	1.7 ± 0.2	1.5 ± 0.2
Peak T	0.12 ± 0.01 [d]	0.30 ± 0.05 [d]	1.2 ± 0.1 [d]
Fe(II) ($\mu mol\ L^{-1}$)	0.5 ± 0.1	4.3 ± 0.7 [c]	0.3
Fe_{total} ($\mu mol\ L^{-1}$)	0.76 ± 0.08 [d]	8 ± 1 [d]	3 ± 2 [d]
Cl^- sample number =	*105* [e]		
Cl^- ($\mu mol\ L^{-1}$)	*5.2 ± 0.4* [e]		
SO_4^{2-} sample number =	*132* [e]		
SO_4^{2-} ($\mu mol\ L^{-1}$)	*4.4 ± 0.3* [e]		
NO_3^{2-} sample number =	*215* [e]		
NO_3^{2-} ($\mu mol\ L^{-1}$)	*0.17 ± 0.02* [e]		

397   [a] Water samples were collected surface waters near the Arctic Long–Term Ecological
398   Research (LTER) site at Toolik Lake, Alaska, USA (68° 38' N, 149° 36' W; elevation 720
399   m) between May and August 2012. Mean values and standard errors are reported for all
400   measurements when possible. [b] Kuparuk River, Sagavanirktok River, Toolik Lake, Toolik
401   Inlet Series, Rooftop River, Nanushuk River, Lake NE–14, and Lake 395. [c] One group
402   significantly different from other two, $p < 0.005$. [d] All groups significantly different, $p <$
403   0.005. [e] Reference 20.
404

405   *Hydroxyl radical formation, quenching, concentration, and quantum yield*

406   Rates of •OH formation ranged from $2.6 \pm 0.6 \times 10^{-12}$ M s^{-1} to $900 \pm 100 \times 10^{-12}$ M s^-

407   ^{1} (Figure 1a) and rate constants of •OH quenching were $5.6 \pm 0.7 \times 10^5$ s^{-1} to $80 \pm 20 \times 10^5$ s^-

408   ^{1} (Figure 1b) The steady–state •OH concentration ($[•OH]_{ss}$) ranged from $2 \pm 1 \times 10^{-17}$ M to

409    $290 \pm 60 \times 10^{-17}$ M (Figure 1c). The $\phi_{•OH}$ values (from 340–410 nm) ranged from 0.06 ± 0.01

410   to $1.8 \pm 0.2 \times 10^{-4}$ (Figure 1d). The rates of •OH formation and quenching, associated •OH

411   steady–state concentrations and apparent quantum yields overlapped with values

412　　previously reported in freshwaters.[15,16,24,63,64]

413

414　　*Spatial and temporal patterns in hydroxyl radical production*

415　　　　Water from Imnavait Creek, a high DOC and iron stream, had the highest rates of

416　　•OH formation, highest steady–state concentrations, and highest apparent quantum yields

417　　(Figure 1). Using ANOVA analysis with a Tukey–Kramer test, the rate of •OH formation

418　　and the steady–state •OH concentration from Imnavait Creek was significantly higher in

419　　comparison to all other lakes, rivers, and streams ($p < 0.01$ and $p < 0.05$, respectively). In

420　　comparison with Imnavait Creek, waters collected from reference or thermokarst soil

421　　waters exhibited lower rates of •OH formation, •OH steady state concentrations, and

422　　apparent quantum yields (Figure 1). Thermokarst soil waters had significantly higher

423　　mean •OH quenching rate constants (Figure 1) compared to the other lakes, rivers, and

424　　streams as determined by ANOVA analysis with a Tukey–Kramer test ($p < 0.001$).

425　　Although Imnavait Creek water had higher rates of •OH formation and lower •OH

426　　quenching compared to thermokarst soil waters, we could not evaluate whether these

427　　differences were statistically significant due to the low number of independent samples

428　　from each water type.

429

430

431
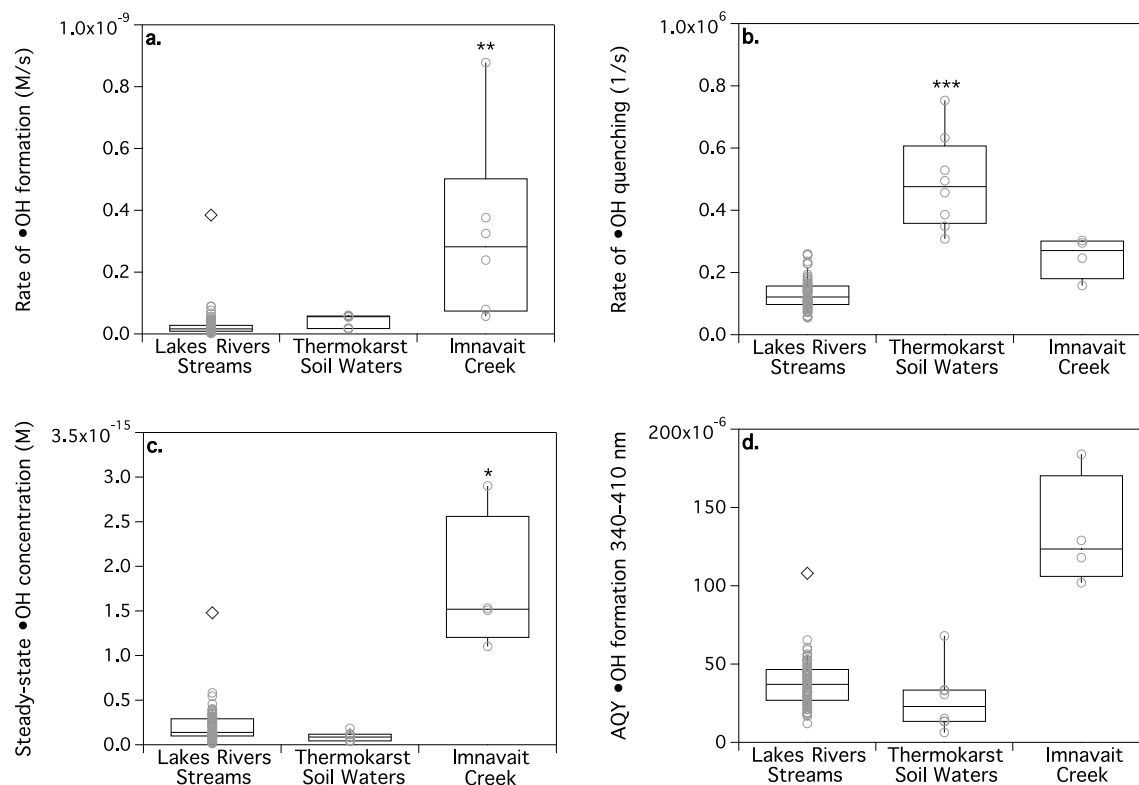
432

433

434 **Figure 1.** Trends in hydroxyl radical formation, quenching, steady–state concentrations,

435 and apparent quantum yield by water type 1) lakes, rivers, and streams, 2) thermokarst

436 soil waters, and 3) Imnavait Creek, a first–order beaded stream. Box–and–whiskers plots

437 of the rate of hydroxyl radical formation ($k_{form,•OH}$, M s^{-1}; 2a), the rate constant of

438 hydroxyl radical quenching ($k_{quench,•OH}$, s^{-1}; 2b), the steady–state concentration of

439 hydroxyl radical ($[•OH]_{ss}$, M; 2c), and the apparent quantum yield of hydroxyl radical

440 formation (AQY; 2d) versus water type. The Kuparuk River early season data point in the

441 lakes, rivers, and streams category is noted in a different symbol. Significant differences

442 between a water type and the lakes, rivers, and streams samples are denoted with *, where

443 * represents $p < 0.05$, ** represents $p < 0.01$, and *** represents $p < 0.001$.

444

445 Comparing the branches of the Inlet Series streams with and without lakes,

446 steady–state concentrations were higher in along the branch without lakes compared to

447 lake outlets by a factor of 3±1 (3.2±0.3x10^{-16} M versus 1.4±0.5x10^{-16} M; Figure 2). Along

20

448　the branch of the stream passing through lakes, the steady–state concentrations were an

449　average of 3±1 times higher at a lake inlet compared to the outlet of the same lake

450　(calculated for I-3, I-5, I-6 headwaters, I-6, and I-Swamp; Figure 2). These differences in

451　steady–state •OH concentrations were primarily driven by differences in rates of •OH

452　formation, because quenching rate constants for •OH were similar at all sites (1.4±0.2

453　$\times 10^5$ s^{-1}).

454　　　　　Steady–state •OH concentrations decreased with increasing distance from the

455　headwaters along the branch of the Inlet Series stream connected by lakes within the

456　Toolik Lake catchment. Steady–state •OH concentrations decreased from a maximum

457　value of 60±10 $\times 10^{-17}$ M at the I–6 inlet to a minimum of 9.6±0.8 $\times 10^{-17}$ M at the I–1

458　outlet (Figure 2), a decrease of ~ 85% over the 18 km distance from the headwater stream

459　to Toolik Lake. As above for differences between lake inlets and outlets, the spatial

460　patterns in steady–state •OH concentrations were primarily driven by differences in rates

461　of •OH formation, because quenching rate constants of •OH were similar at all sites

462　(1.4±0.2 $\times 10^5$ s^{-1}). In contrast, in the branch of the Inlet Series stream without lakes,

463　steady–state concentrations did not decrease significantly over the same length, with a

464　maximum of 34±4 $\times 10^{-17}$ M at the I–8 headwaters and a minimum of 30±1 $\times 10^{-17}$ M at

465　the most downstream site I–8 into I–9 (Figure 2).

466　　　　　Similar to the Inlet Series of lakes and streams, steady–state concentrations of

467　•OH decreased by ~ 80% over the 350 km distance of the river from 31±3 $\times 10^{-18}$ M at the

468　headwaters to 7±2 $\times 10^{-18}$ M at the mouth at the Arctic Ocean (Figure 2). The downstream

469　difference observed in steady–state •OH concentrations in the Kuparuk River was

470　primarily driven by differences in rates of •OH formation given similar rate constants of

471　quenching (8±2 $\times 10^4$ s^{-1}) at all sites with the exception of location 3a, where the rate

472　constant of quenching was double the rate constants observed at all other stations.
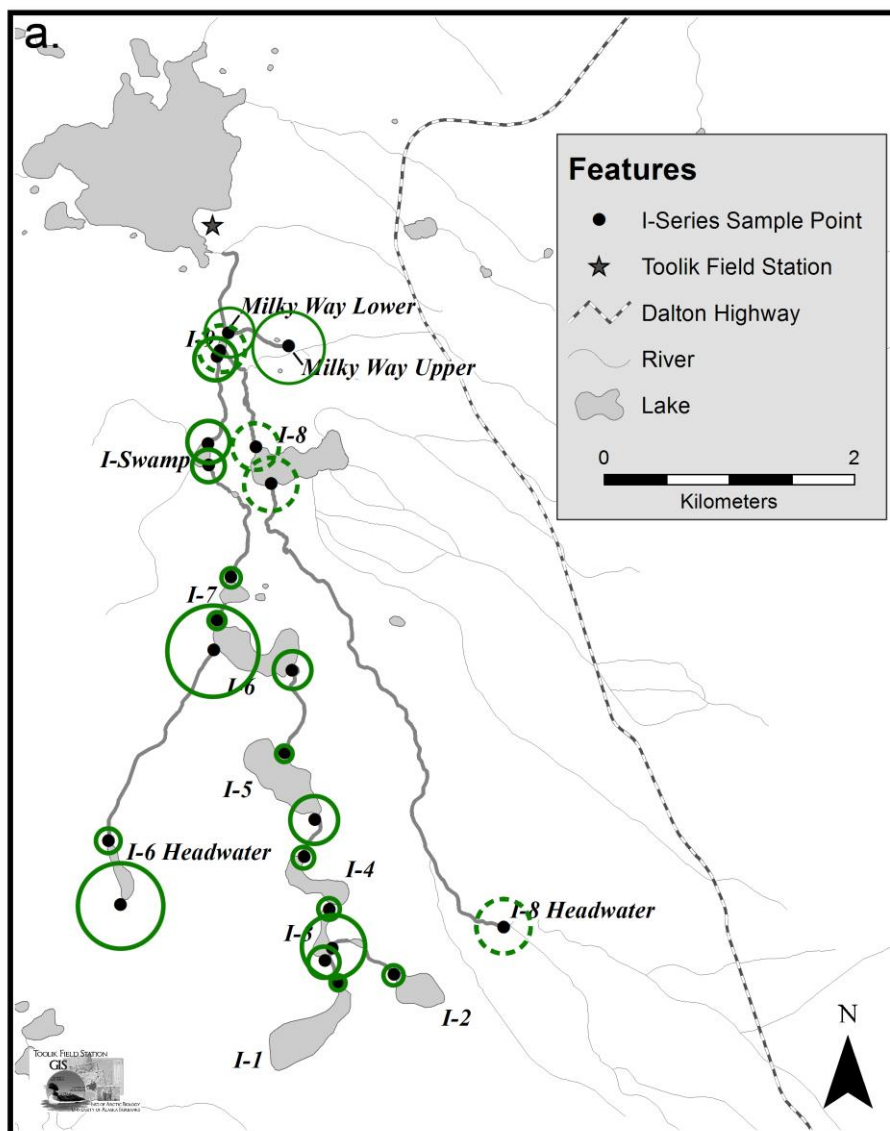
473
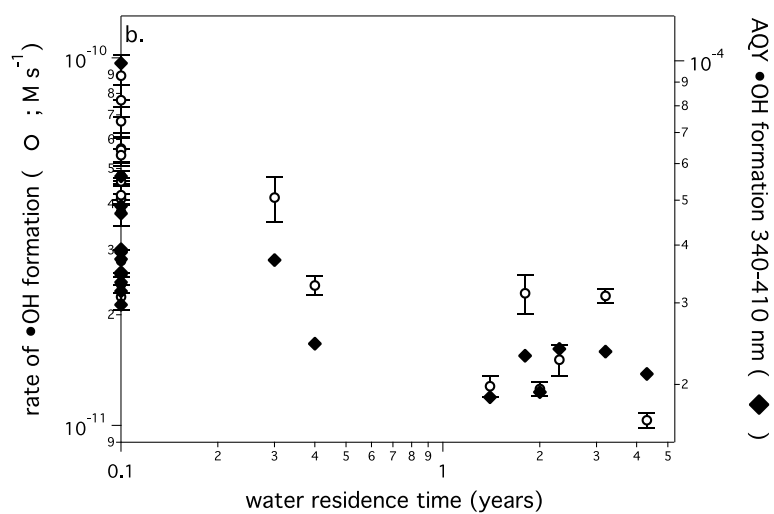
474
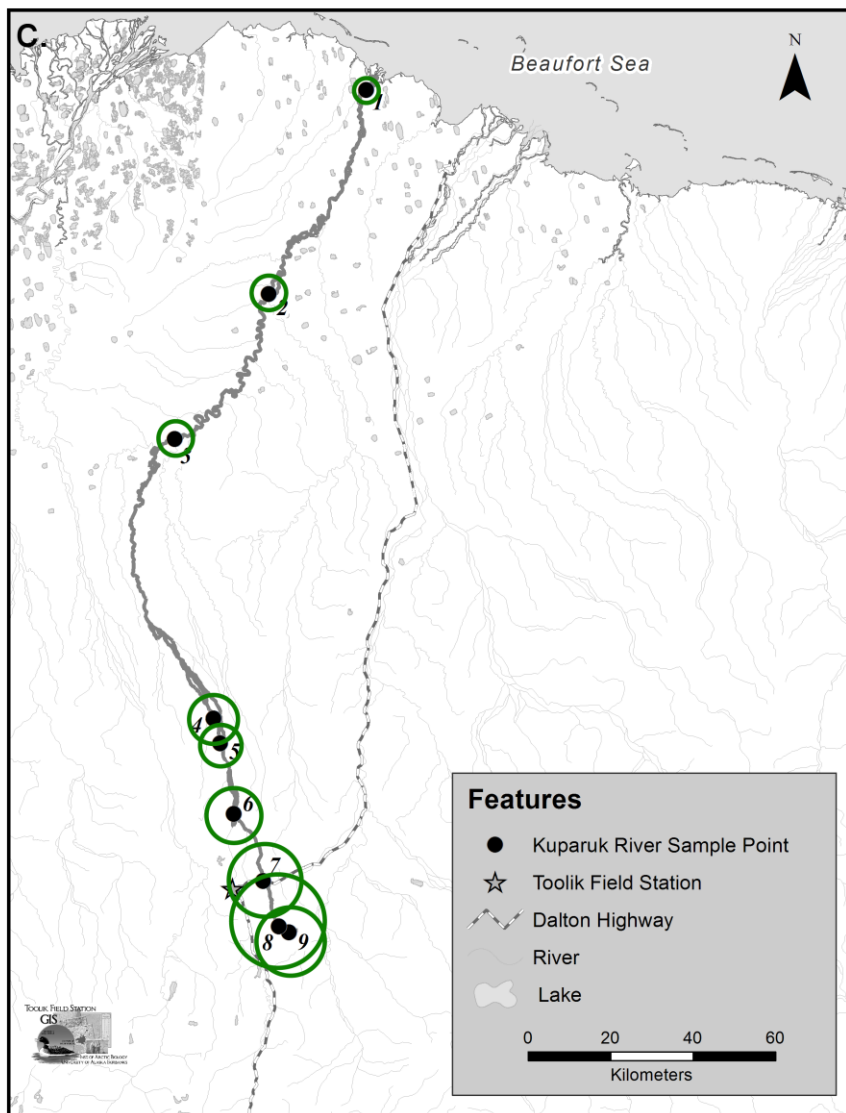
475
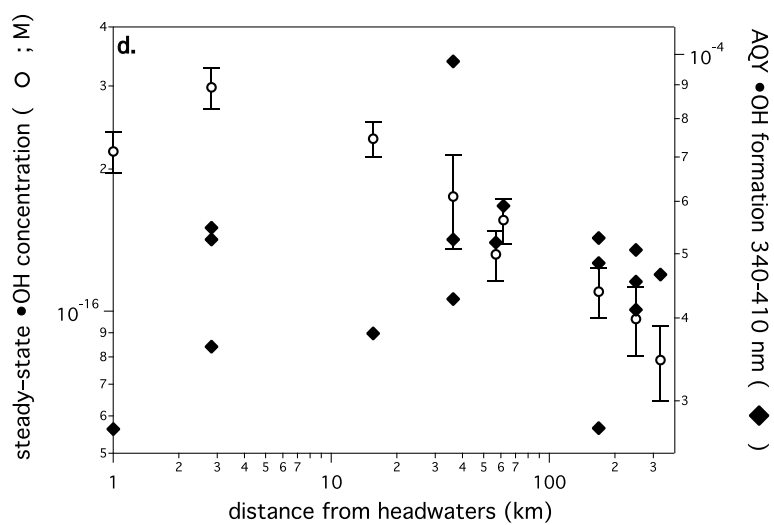
476

477

478

479   **Figure 2.** Spatial variability of hydroxyl radical formation in connected streams and lakes

480   at different spatial scales. (a) Steady–state hydroxyl radical concentrations measured for

481   the Inlet Series of connected streams and lakes in the Toolik Lake catchment sampled on

482   7 and 8 August 2012. The Inlet Series branch with no lakes is denoted by dashed circles,

483   while the branch with lakes and streams is denoted by solid circles. The steady–state

484   hydroxyl radical concentrations in the Inlet Series samples ranged from 9.6 ± 0.8 to 60 ± 10

485     $\times10^{-17}$ M (small to large circles; diameter is proportional to •OH steady–state

486   concentration). (b) Rate of •OH formation (open circles) and apparent quantum yield of

487   •OH formation (filled diamonds) versus water residence time for the I–series samples on

488   7 and 8 August 2012. Water residence times were taken from Kling et al.[20] (c) Steady–

489   state hydroxyl radical concentrations measured for the Kuparuk River sampled on 1

490   August 2012. The steady–state hydroxyl radical concentrations in the Kuparuk River

491   ranged from 7 ± 2 to 31 ± 3 $\times10^{-18}$ M (small to large circles). (d) Steady–state hydroxyl

492   radical concentrations (open circles) and apparent quantum yield of •OH formation (filled

493   diamonds) versus distance from the headwaters for the Kuparuk River sampled on 1

494   August 2012.

495

496   Water collected in May and early June during snowmelt had higher rates of •OH

497   formation, higher steady–state concentrations, and higher apparent quantum yields

498   compared to waters sampled during the summer (Figure 3). For example, in the Toolik

499   Inlet stream, on the 18th, 19th, and 21st of May, 2012, the rates of •OH formation were

500   1.1 ± 0.2, 9.0 ± 0.7, and 1.8 ± 0.1 $\times10^{-11}$ M s^{-1}, respectively. Similarly in the Kuparuk River,

501   on the 18th and 22nd of May, 2012, the rates of •OH formation were 6.3 ± 0.2 and 77 ± 8

502     $\times10^{-11}$ M s^{-1}, respectively, higher than formation rates measured at the same site later in

503   the season (avg. 2.6 ± 0.7 $\times10^{-11}$ M s^{-1}).

504   *Correlation of water quality parameters with hydroxyl radical formation and quenching*

505   Hydroxyl radical formation and quenching were strongly, positively correlated

506   with DOM quantity and quality (e.g., DOC concentration, a_{320}, and peak A, C and T

507   fluorescence intensities; Figs. 3 and 4, Table 2). Stronger correlations between DOM and

508   •OH quenching were observed compared to •OH formation, but the significance of this

509   difference was impossible to evaluate given the lower number of samples (n = 67 vs. n =

510   96; Figures 3 and 4). Formation of •OH was weakly, positively correlated with total iron

511   (R^2 = 0.34, p < 0.05; Figure 3).

512

513
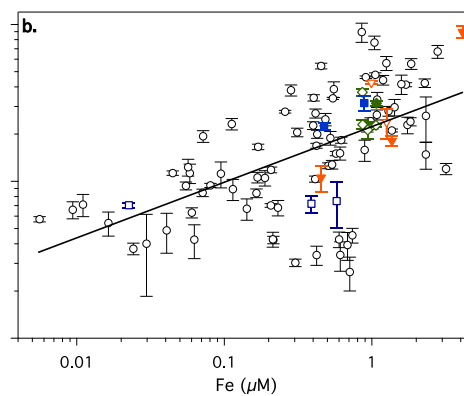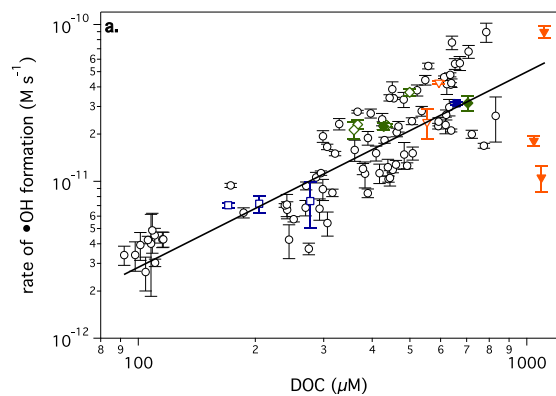
514
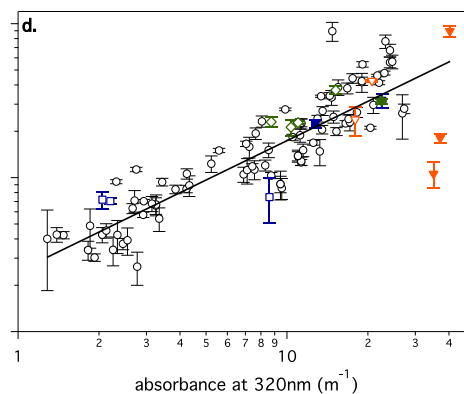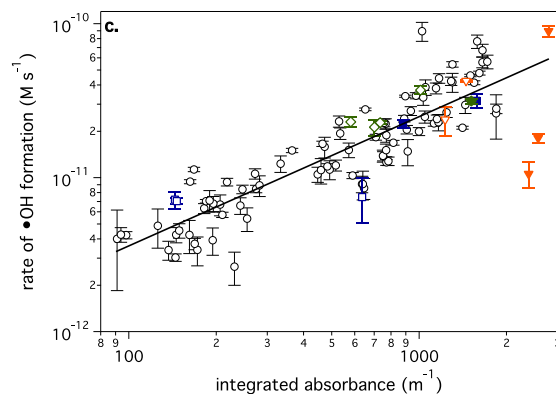
515
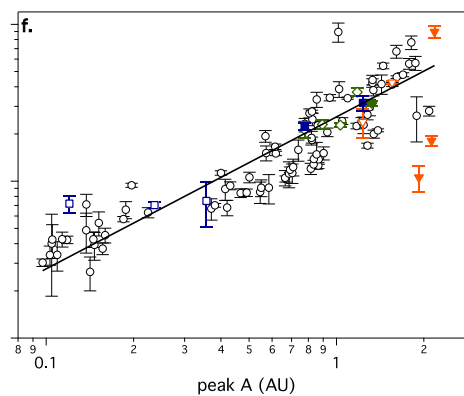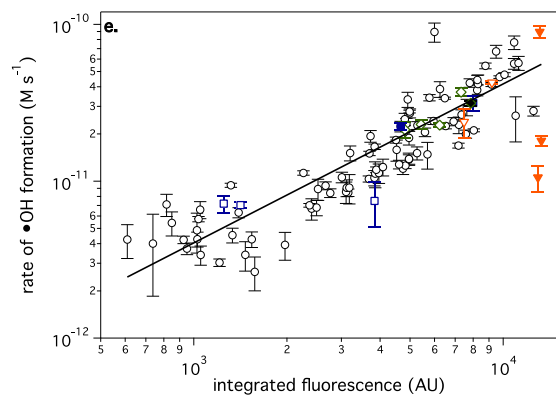
516
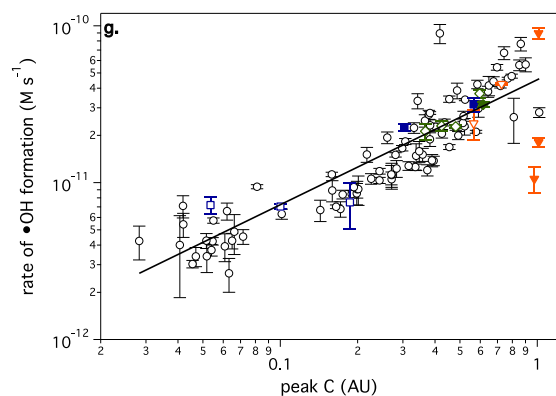
517 **Figure 3.** Scatter plots showing significant correlations between rates of hydroxyl radical

518 formation ($k_{form,•OH}$, M s^{-1}) and water chemistry for samples from lakes, rivers, and

519 streams: DOC (a), total Fe (b), integrated absorbance (c), absorbance at 320 nm (d),

520   integrated fluorescence (e), peak A (f), and peak C (g). Measurements from lakes, rivers,

521   and streams are designated by open circles; measurements from Imnavait Creek and

522   thermokarst soil waters were excluded from the correlations. Measurements from the

523   Kuparuk River (green diamonds), the Sagavanirktok River (blue squares), and the Toolik

524   Inlet (orange triangles) are shown for early season (filled) and summer (open). Fit

525   parameters are as follows: (a) $R^2 = 0.47$, n=96; (b) $R^2 = 0.34$, n=95; (c) $R^2 = 0.53$, n=101;

526   (d) $R^2 = 0.53$, n=101; (e) y = $R^2 = 0.56$, n=101; (f) y = $R^2 = 0.57$, n=101; (g) $R^2 = 0.58$,

527   n=101. All slopes were significantly greater than zero ($p < 0.05$).

528
529

530

531

532

533
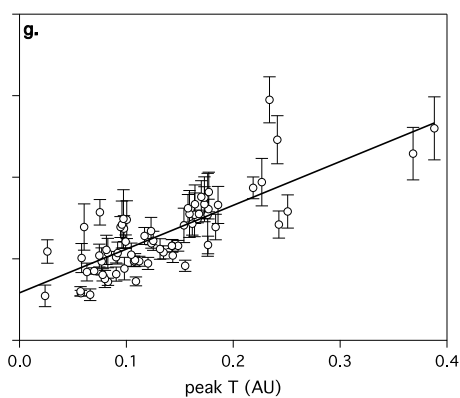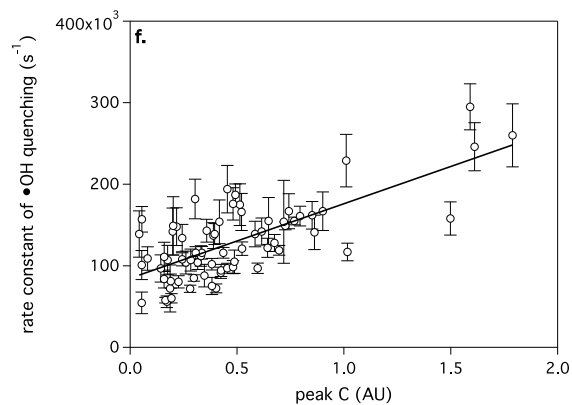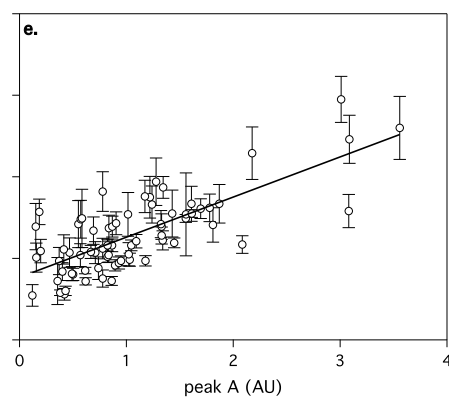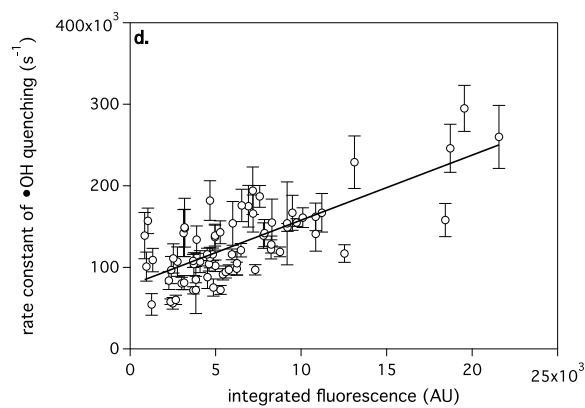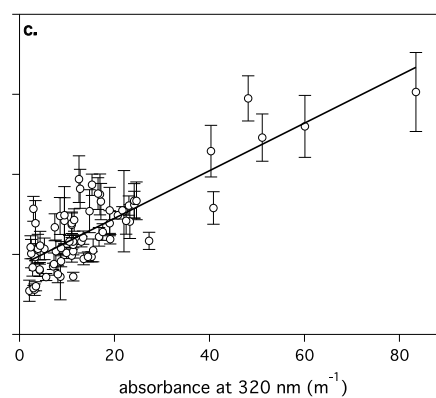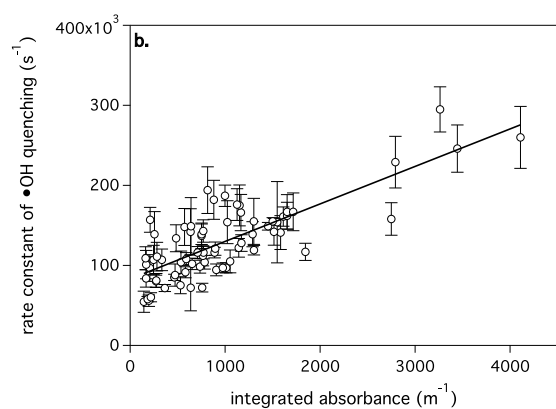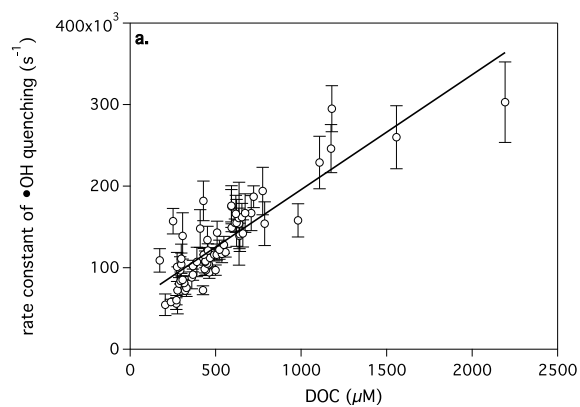
534   **Figure 4.** Scatter plots showing significant correlations between the rate constant of

535   hydroxyl radical quenching ($k_{quench, \cdot OH}$, s^{-1}) and water chemistry: DOC (a), integrated

536   absorbance (b), absorbance at 320 nm (c), integrated fluorescence (d), peak A (e), peak C

537   (f), and peak T (g). Measurements from lakes, rivers, and streams and Imnavait Creek are

538   designated by dark circles; measurements from thermokarst soil waters were excluded

539   from the correlations. Fit parameters are as follows: (a) $R^2 = 0.75$, n=67; (b) $R^2 = 0.63$,

540   n=70; (c) $R^2 = 0.68$, n=71; (d) $R^2 = 0.54$, n=70; (e) $R^2 = 0.56$, n=70; (f) $R^2 = 0.51$, n=70;

541   (g) $R^2 = 0.64$, n=70. All slopes were significantly greater than zero ($p < 0.05$).

542

543

544   **Discussion**

545   *Iron is a source of •OH in arctic surface waters*

546   Several lines of evidence suggested that iron contributed to the photochemical

547   production of •OH in arctic surface waters. First, across the range of relatively high iron

548   concentrations in the surface water studied (~ 0.8 – 8 μM total Fe; Table 1), iron

549   concentration was significantly, positively correlated with •OH formation (Figure 3)

550   consistent with previous work showing iron was also positively correlated with •OH

551   production.[23] It was likely that iron contributed to •OH formation through the photo−

552   Fenton reaction, given that the highest •OH production and steady state concentrations

553   were observed in Imnavait Creek (Table 1), in which the low pH and high iron waters are

554   conducive to this reaction.[2] Although the contribution of iron to •OH formation through

555   the photo−Fenton reaction may not scale in proportion to the concentration of Fe,

556   concentrations as low as 80 nM of iron have been estimated to initiate photo−Fenton

557   reactions in natural waters.[4] However, iron concentrations were also correlated with

558   concentrations and quality of DOM (e.g. DOC, CDOM, and FDOM, R^2 = ~ 0.5, p < 0.05,

559   data not shown), and •OH production was most strongly correlated with measures of the

560   concentration of chromphoric DOM (e.g. $a_{CDOM,\lambda}$ and FDOM; Figure 3). Thus it was not

561   possible to untangle the relative contribution of iron or DOM to •OH based only on the

562   observed correlations.

563

564   *DOM is the primary source and sink of •OH in arctic surface waters*

565   Several lines of evidence strongly supported DOM as an important source and sink

566   for •OH in arctic surface waters: temporal and spatial patterns of •OH production were

567   related to biogeochemical processes that control the concentration and chemical

568   composition of chromophoric DOM, and •OH quenching was most strongly correlated

569   with the concentration and chemical composition of chromophoric DOM. In addition to

570   correlative evidence from temporal and spatial gradients in DOC, CDOM, FDOM, and

571   •OH, comparison of the yields of •OH in arctic surface waters to other studies suggested

572   that the DOM, especially in small arctic streams, was better at making •OH relative to

573   DOM in other surface waters with comparable iron concentrations.

574   <u>Hydroxyl radical production is correlated with DOM</u>

575   Of the measures of DOM quantity and quality tested, •OH production was most

576   strongly correlated with CDOM and FDOM, proxies for the light–absorbing,

577   chromophoric fraction of DOM associated with aromatic carbon from degrading lignin.

578   For example, •OH production was strongly positively correlated with fluorescence peaks

579   A and C (Figure 3) but not with peak T. In arctic surface waters, peaks A and C have

580   been correlated with measures of terrestrially–derived organic matter enriched in

581   aromatic carbon, while peak T was correlated with proxies of amino acid–like carbon

582   (e.g. %N and δ^{15}N).[32] Aromatic CDOM is the main light–absorbing constituent in

583   freshwaters, including the surface waters near Toolik Lake[65,66] and as such initiates

584   photochemical reactions of DOM. Correlation of •OH production with the light–

585   absorbing fraction of DOM that initiates photochemical reactions is consistent with

586   previous work showing that the fulvic acid fraction of DOM from Toolik Lake with the

587   highest aromatic carbon content produced the most photochemical •OH[67] and with studies

588   suggesting that direct photolysis of the aromatic fraction of DOM was a pathway for the

589   photochemical production of •OH in natural waters.[15,17] Given that CDOM and FDOM

590   are better proxies for the concentration of aromatic compared to bulk DOC

591   concentrations, it was not surprising that this and previous studies have reported stronger

592   relationships between •OH production with CDOM and FDOM compared to DOC.

593   Furthermore, Sharpless et al. found that •OH production from DOM was correlated to the

594   capacity of the DOM to donate electrons.[26] This electron donating capacity (EDC) of

595   DOM is correlated with phenol content,[68] which comprises a large portion of the aromatic

596   moieties of aquatic DOM.[69,70]

597   <u>Seasonal and longitudinal gradients in •OH are linked to controls on CDOM</u>

598   **Light exposure decreases •OH formation** The seasonal and longitudinal patterns

599   in DOC, CDOM, FDOM, and •OH production showed that •OH production was highest

600   from terrestrial organic matter enriched in aromatic carbon with little prior light exposure,

601   and that •OH production decreased as this DOM was increasingly modified in streams

602   and lakes. For example, highest rates of •OH production were observed from waters

603   where the DOM had the lowest level of prior light exposure, such as Imnavait Creek

604   (Figure 1), a first–order stream draining organic soils rich in aromatic carbon with little

605   previous light exposure.[32] DOM in thermokarst soil waters has also likely had little prior

606   light exposure,[34] but these waters have less chromophoric (aromatic) carbon per DOC,[34]

607   consistent with the proportionally lower formation of •OH from thermokarst soil waters

608   compared to CDOM–rich Imnavait Creek.

609   In addition, at a given site, •OH production was significantly higher from waters

610   collected during snowmelt in early spring compared to samples collected from the same

611   site during mid–summer (Figure 3). Increasing light exposure with increasing residence

612   time of terrestrially–derived DOM in sunlit surface waters of the Arctic has been shown

613   to break down the chromophoric aromatic moieties in DOM, i.e. photobleaching of

614   CDOM.[32] Photobleaching is a sink for CDOM,[71,72] consistent with earlier findings

615   showing that •OH production also decreases with increasing light exposure.[6,15,26]

616   Together, these studies suggest that photodegradation removes or alters the aromatic

617   CDOM moieties associated with •OH production. As CDOM is increasingly degraded by

618   sunlight in surface waters, the remaining CDOM is less effective at producing •OH.

619   While •OH production was significantly higher from waters collected during

620   snowmelt in early spring compared to samples collected from the same site during mid−

621   summer, stream waters collected from the same site over consecutive days during

622   snowmelt exhibited large variability in •OH concentrations (Figure 3). It was not possible

623   to statistically resolve the relative importance of iron vs. DOM in the observed variability

624   in •OH during this period given the low number of samples and the fact that DOM and

625   iron were themselves correlated. However, qualitatively, the early season variability in

626   •OH appeared to be best explained by iron concentrations compared to measures of DOC,

627   CDOM or FDOM (Figure 4).

628   Further evidence in support of sunlight as a sink for the moieties in CDOM

629   associated with •OH production was the 80% decrease in •OH formation along the 18 km

630   distance downstream in the branch of the Inlet Series stream containing lakes, in contrast

631   to no detectable decrease along the same distance downstream in the branch without

632   lakes. Given the significantly lower •OH formation at lake outlets compared to the

633   respective lake inlet (Figure 2), the net effect of lakes along the inlet course was to

634   consume the potential for •OH formation consistent with the negative correlation between

635   •OH formation or the apparent quantum yield (AQY) of •OH formation and water

636   residence time along the branch of the Inlet Series stream passing through lakes (Figure

637   2). Given that photobleaching of CDOM in arctic surface waters occurs on similar

638   timescales to DOM transit,[32] and that surface waters were collected from the lakes during

639   periods of stratification[20,31,73] when there was little prospect for recharge in CDOM in

640   from bottom waters, the most likely explanation of the removal of CDOM and •OH

641   production with increasing residence time was photochemical degradation of CDOM in

642   the sunlit surface waters.[32] Consistently, AQYs and steady state concentrations of •OH in

643   the Inlet Series stream were strongly, positively correlated with measures of DOM

644   composition altered by photodegradation (e.g. the fluorescence index[32]), but were not

645   correlated with total iron (supplementary Figure S1).

646   Previous work strongly suggested that photochemical degradation of soil-derived

647   DOM was largely responsible for the decrease in aromatic C and associated decrease in

648   CDOM and other optical proxies of DOM between streams and lakes differing in water

649   residence times (e.g. 18-23% aromatic C for streams compared to 16-18% for lakes,

650   respectively[32]). While there was likely photodegradation of CDOM and associated loss of

651   •OH production potential with distance downstream in the Inlet Series branch without

652   lakes, inputs of new CDOM from the soil waters likely compensated for CDOM removed,

653   resulting in no detectable loss of •OH production potential along the 18 km transect

654   downstream (Figure 2).

655   In comparison to small streams, inputs of terrestrial C have a smaller impact on

656   the chemistry of DOM in larger rivers like the Kuparuk River, as the DOM moves

657   downstream especially under low–flow conditions when the river was sampled in August,

658   2012 (Figure 2). Thus, the roughly linear decrease in •OH formation with distance

659   downstream along the 350–km transect of the Kuparuk River from its headwaters to the

660   mouth at the Arctic Ocean (Figure 2) was likely due to a loss of CDOM or dilution with

661   similar sources of CDOM. This is because in contrast to observations in the I–series

662   (Figure 2), the AQY of •OH formation was relatively constant down the length of the

663   Kuparuk River (Figure 2), indicating that although the concentration of DOM was

664   decreasing the DOM was not changing in its ability to make •OH with distance

665   downstream. The similar percent decrease in •OH formation (~ 80%) across spatial scales

666   differing by an order of magnitude, i.e. 18 km in the Inlet Series stream with connected

667   lakes and streams compared to the 350 km stretch of the Kuparuk River, was likely due to

668   the orders of magnitude longer residence time of water and DOM in lakes of the Inlet

669 Series than in the Kuparuk River,[20,32] resulting in greater degradation of •OH–forming

670 DOM in the Inlet Series compared to the Kuparuk River.

671 **High aromatic content and low prior light exposure increase •OH formation**

672 **potential** As previously discussed, •OH production rates were highest in Imnavait Creek,

673 a naturally acidic headwater stream draining waterlogged organic soils rich in DOM and

674 iron. Rates of •OH production in Imnavait Creek were greater than the range reported

675 from acid mine drainage waters (AMD; $440 - 7400 \times 10^{-12}$ M s^{-1}), despite $36 - 3800$

676 times less iron and higher pH in Imnavait Creek compared to AMD waters (Imnavait: pH

677 5.2; AMD: pH $2 - 3$).[74] In addition, rates of •OH production in Imnavait Creek were

678 greater than rates in river waters where nitrate and nitrite were important sources of •OH.

679 These rivers were impacted by agricultural or urban run–off and had more than 450 times

680 more nitrate ($78 - 197$ μM) and nitrite ($3.4 - 34$ μM)[23,24] compared to Imnavait Creek and

681 the other surface waters studied where concentrations of nitrate/nitrite could account for

682 only a trace fraction of •OH observed.[17] Finally, rates of •OH production in Imnavait

683 Creek overlapped rates of •OH production in freshwaters with similar pH and DOC

684 concentration ($450 - 1700 \times 10^{-12}$ M s^{-1}), but at least ~10 times higher nitrate and ~1000

685 times higher iron concentrations to Imnavait Creek.[3,15] Hydroxyl radical steady state

686 concentrations in Imnavait Creek were also higher than steady–state concentrations

687 reported for a range of freshwaters (average $180 \pm 70 \times 10^{-17}$ M, max $290 \pm 60 \times 10^{-17}$ M vs.

688 $0.1 - 84 \times 10^{-17}$ M).[15,16,63] Only AMD waters had higher steady state concentrations of •OH

689 than Imnavait Creek ($670 - 400000 \times 10^{-17}$ M)[74] consistent with their much higher

690 concentrations of iron compared to Imnavait Creek.

691 Thus, •OH production and steady state concentrations from Imnavait Creek waters

692 were the same magnitude as waters with much greater concentrations of "other" (non–

693 DOM) sources of photochemical •OH (e.g. iron, nitrate, nitrite in the AMD, agriculturally

694   impacted waters, or coastal or blackwater swamps). Given the disproportionately high

695   rates of •OH production in Imnavait Creek despite much lower concentrations of non–

696   DOM sources of •OH (e.g. iron, nitrate, nitrite), the chemical attributes of the DOM, or of

697   the DOM and iron together, may be particularly effective at •OH production in Imnavait

698   Creek and similar headwater streams draining organic rich soils compared to other

699   surface waters.

700   While comparison of rates of production and steady state concentrations of •OH in

701   arctic surface waters to other studies suggested that the DOM or iron may be more

702   effective as a source of •OH, the real test of increased capacity to form •OH is the AQY

703   for •OH formation, which corrects for different rates of light absorption among waters.

704   Because the quantum yields in this study were measured at a longer wavelength (365 nm)

705   than previously reported, a direct comparison of quantum yields was not possible.

706   However, assuming that the natural waters in this study had a similar wavelength–

707   dependence of •OH quantum yield as reported for the aquatic reference DOM SRFA,[17]

708   the quantum yield at 310 nm would be ~ 0.2–7×10^{-4}, within the range of what has

709   previously been reported from 300–340 nm in coastal and river waters with much higher

710   concentrations of iron and nitrate/nitrite compared to arctic surface waters.[3,17] Because

711   the contribution of DOM to the apparent quantum yields in other waters had to be lower

712   than in arctic surface waters (due to the much higher concentrations of iron, nitrate, and

713   nitrite) [3,17] our hypothesis is that the amount and the chemical composition of aromatic

714   DOM, or perhaps the CDOM and iron together, makes CDOM in small, first order

715   streams like Imnavait Creek more effective at producing •OH.

716   Because the detailed mechanism for photochemical formation of •OH from DOM

717   is not known, it is difficult to speculate on the chemical attributes of aromatic CDOM

718   (alone or with iron) that effect •OH formation. It seems apparent that the best sources of

Environmental Science: Processes & Impacts

719   •OH are the aromatic C moieties most labile to photochemical degradation, given that the

720   highest rates of •OH production were associated with freshly flushed soil material

721   enriched in aromatic DOM, and that there was rapid loss of •OH formation within several

722   km of travel time downstream or within short residence times (Figure 2), consistent with

723   the previously observed decrease in aromatic C content with increasing water residence

724   times in these waters.[32] In addition to the amount of aromatic C, the chemical

725   composition of aromatic C (alone or with iron), may also influence the production of •OH

726   from DOM. Imnavait Creek water had 3-7 fold higher AQY for •OH production

727   compared to Suwannee River DOM (2.7×10^{-5} compared to ~ 2.7×10^{-4}), despite similar

728   amounts of aromatic C (22-24%[32]). However, there was likely higher iron concentration

729   in Imnavait Creek water compared to the isolate of Suwannee River DOM, which may

730   account for the higher AQY of •OH formation in this case. Although we are unable to

731   determine the relative importance of aromatic C content, composition or iron

732   concentration in this study, together in comparison to Suwannee River DOM and to

733   waters elevated in nitrate, nitrite, and iron, our results imply that the combination of

734   DOM and iron in arctic streams may be relatively more effective at making •OH, and thus

735   •OH formation and likely its role as an oxidant of organic carbon may be highest in first–

736   order streams like Imnavait Creek.

737   Hydroxyl radical quenching is correlated with DOM

738   Quenching of •OH has been attributed to DOM in freshwaters and to anions,

739   especially in seawater, that then form radical species of lower energy and higher reaction

740   selectivity. Like other low conductivity freshwaters, DOM was likely the most important

741   sink for •OH in arctic surface waters for two reasons. First, the highest quenching rate

742   constants were observed in high–DOM waters (Table 1, Figure 1) and quenching was

743   strongly correlated with measures of DOM concentration (DOC, CDOM, FDOM; Figure

744   4). Normalized per mole of C, the rate constants of •OH quenching ($3\pm2 \times10^8$ M_C^{-1} s^{-1})

745   were well within the range reported for DOM (1.6–12 $\times10^8$ M_C^{-1} s^{-1}).[75-77] Second, the

746   freshwaters of the Arctic contained low concentrations of quenching anions (e.g. chloride

747   and bromide) associated with high rates of •OH scavenging reported in seawaters, where

748   concentrations chloride and bromide are in the 100's of mM.[64]

749   The highest observed quenching rate constant of $80\pm20 \times10^5$ s^{-1} was observed in

750   thermokarst soil waters, three– to four–fold higher than the highest rates reported from

751   freshwater[3] or seawater.[64] Thermokarst soil waters contained high levels of carbonate

752   (alkalinity 1700 ± 1600 µeq L^{-1}), which could react with •OH at a slower rate than with

753   organic compounds (8.5×10^6 M^{-1} s^{-1} for carbonate, versus an average 10^8 M_C^{-1} s^{-1} for

754   organics).[28] However, DOC concentrations were on average three–fold greater than

755   carbonate concentrations (Table 1). Further, when normalized by DOC concentration, the

756   quenching rate in thermokarst soil waters was similar to the other surface waters (1.9±0.2

757    $\times10^8$ M_C^{-1} s^{-1}). These results, together with a lack of correlation between the rate of •OH

758   quenching and carbonate alkalinity, suggest that even in thermokarst soil waters, DOM

759   was the major sink for •OH.

760   *The implications of •OH production for arctic carbon cycling*

761   Given that DOM was most likely the predominant source and sink for •OH in

762   arctic waters, the fate of •OH is likely to oxidize DOM. Because •OH is known to react

763   with DOM to yield CO_2,[5,78] we estimated the potential contribution of •OH to the

764   photomineralization of DOM (i.e. photochemical production of CO_2). Given that apparent

765   quantum yields for photomineralization from freshwater DOM are 10–100 times greater

766   than apparent quantum yields of •OH production,[3,79] and assuming a yield of 0.3 mol CO_2

767   per mol •OH,[5] we estimated that •OH could contribute ~ 0.04–4% of total

768   photomineralization in these waters, consistent with previous studies that have similarly

769   estimated the contribution of •OH to photomineralization of DOM.[1,5,6] The contribution

770   of •OH to photo–mineralization was highest in the low pH, high iron waters as expected,

771   but even under conditions conducive to photo–Fenton chemistry our observations and

772   estimates suggest that there may not be enough •OH to produce the photochemical CO_2

773   observed.[66]

774   These estimates for the role of •OH in the oxidation of DOM highlight the

775   assumptions and knowledge gaps regarding the importance of •OH as an oxidant in

776   aquatic ecosystems, including the wavelength–dependence of •OH production in natural

777   waters,[3,17,64] the yield of CO_2 per •OH, and the possibility of a microheterogeneous

778   distribution of •OH production in the DOM. First, the wavelength–dependence of •OH

779   production has been characterized from 305 to 360 nm only for a standard DOM isolate

780   (SRFA);[17] the wavelength dependence of •OH production is poorly known in natural

781   waters.[3,17,64] Second, only one study has measured the yield of CO_2 per mol •OH under

782   controlled laboratory conditions in which •OH was produced by pulse radiolysis,[5,6] and

783   this yield may differ in natural waters varying in sources of •OH and in chemical

784   composition of DOM. Finally, there is evidence for microheterogeneous reactivity of

785   DOM,[80-82] in which regions within DOM have been shown to have enhanced

786   concentrations of $^1O_2$[80,82] or to protect hydrophobic molecules from reactions occurring in

787   the bulk solution.[81] If •OH is produced within the DOM microenvironment, then the

788   DOM may experience higher •OH concentrations than measured by the probe in the bulk

789   phase, leading to a systematic under–estimation of •OH contribution to

790   photomineralization. Because addressing each uncertainty listed here could increase the

791   contribution of •OH in the photomineralization of DOM, further work is needed to assess

792   the role of •OH in photomineralization of DOM in arctic surface waters, especially in

793   first–order streams like Imnavait Creek where •OH formation was highest. First order

794   streams like Imnavait Creek are common to the North Slope of Alaska[83] and are

795   important in the processing of DOM in higher–order streams,[66] thus future work will be

796   aimed at addressing the role of •OH as an oxidant of DOM in these streams.

797

803

804   **Author Information.** Correspondence and requests for materials should be addressed to

805   K.M.: email, kris.mcneill@env.ethz.ch; phone, +41 44 632 47 55; fax, +41 44 632 14 38; and

806   R.M.C.: email, rmcory@umich.edu; phone, +1 734 615 3199; fax, +1 734 763 4690.

41

807   **References**

808   (1) Molot, L. A.; Hudson, J. J.; Dillon, P. J.; Miller, S. A. Effect of pH on Photo-

809   Oxidation of Dissolved Organic Carbon by Hydroxyl Radicals in a Coloured, Softwater

810   Stream. *Aquat. Sci.* **2005**, 67, 189.

811   (2) Southworth, B. A.; Voelker, B. M. Hydroxyl radical production via the photo-Fenton

812   reaction in the presence of fulvic acid. *Environ. Sci. Technol.* **2003**, 37, 1130.

813   (3) White, E. M.; Vaughan, P. P.; Zepp, R. G. Role of the Photo-Fenton Reaction in the

814   Production of Hydroxyl Radicals and Photobleaching of Colored Dissolved Organic

815   Matter in a Coastal River of the Southeastern United States. *Aquat. Sci.* **2003**, 65, 402.

816   (4) Vermilyea, A. W.; Voelker, B. M. Photo-Fenton reaction at near neutral pH. *Environ.*

817   *Sci. Technol.* **2009**, 43, 6927.

818   (5) Goldstone, J. V.; Pullin, M. J.; Bertilsson, S.; Voelker, B. M. Reactions of hydroxyl

819   radical with humic substances: Bleaching, mineralization, and production of bioavailable

820   carbon substrates. *Environ. Sci. Technol.* **2002**, 36, 364.

821   (6) Vione, D.; Lauri, V.; Minero, C.; Maurino, V.; Malandrino, M.; Carlotti, M.; Olariu,

822   R.-I.; Arsene, C. Photostability and photolability of dissolved organic matter upon

823   irradiation of natural water samples under simulated sunlight. *Aquat. Sci.* **2009**, 71, 34.

824   (7) Zafiriou, O. C.; True, M. B. Nitrite Photolysis in Seawater by Sunlight. *Mar. Chem.*

825   **1979**, 8, 9.

826   (8) Mack, J.; Bolton, J. R. Photochemistry of Nitrite and Nitrate in Aqueous Solution: A

827   Review. *J. Photochem. Photobiol., A* **1999**, 128, 1.

828   (9) Minero, C.; Chiron, S.; Falletti, G.; Maurino, V.; Pelizzetti, E.; Ajassa, R.; Carlotti,

829   M. E.; Vione, D. Photochemical Processes Involving Nitrite in Surface Water Samples.

830   *Aquat. Sci.* **2007**, 69, 71.

831 (10) Zafiriou, O. C.; True, M. B. Nitrate Photolysis in Seawater by Sunlight. *Mar. Chem.*

832 **1979**, 8, 33.

833 (11) Zepp, R. G.; Hoigné, J.; Bader, H. Nitrate-Induced Photooxidation of Trace Organic

834 Chemicals in Water. *Environ. Sci. Technol.* **1987**, 21, 443.

835 (12) Brekken, J. F.; Brezonik, P. L. Indirect Photolysis of Acetochlor: Rate Constant of a

836 Nitrate-Mediated Hydroxyl Radical Reaction. *Chemosphere* **1998**, 36, 2699.

837 (13) Brezonik, P. L.; Fulkerson-Brekken, J. Nitrate-Induced Photolysis in Natural Waters:

838 Controls on Concentrations of Hydroxyl Radical Photo-Intermediates by Natural

839 Scavenging Agents. *Environ. Sci. Technol.* **1998**, 32, 3004.

840 (14) Zepp, R. G.; Faust, B. C.; Hoigné, J. Hydroxyl radical formation in aqueous

841 reactions (pH 3-8) of iron(II) with hydrogen peroxide: The photo-Fenton reaction.

842 *Environ. Sci. Technol.* **1992**, 26, 313.

843 (15) Mopper, K.; Zhou, X. L. Hydroxyl radical photoproduction in the sea and its

844 potential impact on marine processes. *Science* **1990**, 250, 661.

845 (16) Zhou, X. L.; Mopper, K. Determination of Photochemically Produced Hydroxyl

846 Radicals in Seawater and Fresh-Water. *Mar. Chem.* **1990**, 30, 71.

847 (17) Vaughan, P. P.; Blough, N. V. Photochemical formation of hydroxyl radical by

848 constituents of natural waters. *Environ. Sci. Technol.* **1998**, 32, 2947.

849 (18) Page, S. E.; Arnold, W. A.; McNeill, K. Assessing the contribution of free hydroxyl

850 radical in organic matter-sensitized photohydroxylation reactions. *Environ. Sci. Technol.*

851 **2011**, 45, 2818.

852 (19) Guerard, J.; Miller, P.; Trouts, T.; Chin, Y.-P. The Role of Fulvic Acid Composition

853 in the Photosensitized Degradation of Aquatic Contaminants. *Aquat. Sci.* **2009**, 71, 160.

854   (20) Kling, G. W.; Kipphut, G. W.; Miller, M. M.; O'Brien, W. J. Integration of lakes and

855   streams in a landscape perspective: the importance of material processing on spatial

856   patterns and temporal coherence. *Freshwater Biol.* **2000**, 43, 477.

857   (21) Meybeck, M. Carbon, nitrogen, and phosphorus transport by world rivers. *Am. J. Sci*

858   **1982**, 282, 401.

859   (22) Mulholland, P. J. In *Aquatic Ecosystems: Interactivity of Dissolved Organic Matter*;

860   Sinsabaugh, S. F. a. R., Ed.; Elsevier Science: 2003, p 139.

861   (23) Nakatani, N.; Ueda, M.; Shindo, H.; Takeda, K.; Sakugawa, H. Contribution of the

862   Photo-Fenton Reaction to Hydroxyl Radical Formation Rates in River and Rain Water

863   Samples. *Anal. Sci.* **2007**, 23, 1137.

864   (24) Takeda, K.; Takedoi, H.; Yamaji, S.; Ohta, K.; Sakugawa, H. Determination of

865   Hydroxyl Radical Photoproduction Rates in Natural Waters. *Anal. Sci.* **2004**, 20, 153.

866   (25) Timko, S. A.; Romera-Castillo, C.; Jaffe, R.; Cooper, W. J. Photo-reactivity of

867   natural dissolved organic matter from fresh to marine waters in the Everglades system of

868   Florida, USA. *Environmental Science: Processes & Impacts* **2014**.

869   (26) Sharpless, C. M.; Aeschbacher, M.; Page, S. E.; Wenk, J.; Sander, M.; McNeill, K.

870   Photooxidation–induced changes in optical, electrochemical, and photochemical

871   properties of humic substances. *Environ. Sci. Technol.* **2014**, 10.1021/es403925g.

872   (27) Brinkmann, T.; Sartorius, D.; Frimmel, F. H. Photobleaching of Humic Rich

873   Dissolved Organic Matter. *Aquat. Sci.* **2003**, 65, 415.

874   (28) Buxton, G. V.; Greenstock, C. L.; Helman, W. P.; Ross, A. B. Critical review of rate

875   constants for reactions of hydrated electrons, hydrogen atoms and hydroxyl radicals

876   (OH/O⁻) in aqueous solution. *J. Phys. Chem. Ref. Data* **1988**, 17, 513.

877   (29) Rember, R. D.; Trefry, J. H. Increased concentrations of dissolved trace metals and

878   organic carbon during snowmelt in rivers of the Alaskan Arctic. *Geochim. Cosmochim.*

879   *Acta* **2004**, 68, 477.

880   (30) Kling, G.; O'Brien, W. J.; Miller, M. C.; Hershey, A. E. In *Toolik Lake*; O‚ÄôBrien,

881   W. J., Ed.; Springer Netherlands: 1992; Vol. 78, p 1.

882   (31) Crump, B. C.; Adams, H. E.; Hobbie, J. E.; Kling, G. W. Biogeography of

883   bacterioplankton in lakes and streams of an arctic tundra catchment. *Ecology* **2007**, 88,

884   1365.

885   (32) Cory, R. M.; McKnight, D. M.; Chin, Y.-P.; Miller, P.; Jaros, C. L. Chemical

886   characteristics of fulvic acids from Arctic surface waters: Microbial contributions and

887   photochemical transformations. *J. Geophys. Res.* **2007**, 112, G04S51.

888   (33) Stubbins, A.; Spencer, R. G.; Chen, H.; Hatcher, P. G.; Mopper, K.; Hernes, P. J.;

889   Mwamba, V. L.; Mangangu, A. M.; Wabakanghanzi, J. N.; Six, J. Illuminated darkness:

890   Molecular signatures of Congo River dissolved organic matter and its photochemical

891   alteration as revealed by ultrahigh precision mass spectrometry. *Limnol. Oceanogr.* **2010**,

892   55, 1467.

893   (34) Cory, R. M.; Crump, B. C.; Dobkowski, J. A.; Kling, G. W. Surface exposure to

894   sunlight stimulates CO_2 release from permafrost soil carbon in the Arctic. *Proc. Natl.*

895   *Acad. Sci.* **2013**.

896   (35) Amon, R. M. W.; Meon, B. The biogeochemistry of dissolved organic matter and

897   nutrients in two large Arctic estuaries and potential implications for our understanding of

898   the Arctic Ocean system. *Mar. Chem.* **2004**, 92, 311.

899   (36) Laurion, I.; Mladenov, N. Dissolved organic matter photolysis in Canadian arctic

900   thaw ponds. *Environmental Research Letters* **2013**, 8, 035026.

901   (37) Zhang, Y.; Chen, W.; Riseborough, D. W. Temporal and spatial changes of

902   permafrost in Canada since the end of the Little Ice Age. *J. Geophys. Res.* **2006**, 111,

903   D22103.

904   (38) Jorgenson, M. T.; Shur, Y. L.; Pullman, E. R. Abrupt increase in permafrost

905   degradation in Arctic Alaska. *Geophysical Research Letters* **2006**, 33.

906   (39) Holmes, R. M.; McClelland, J. W.; Raymond, P. A.; Frazer, B. B.; Peterson, B. J.;

907   Stieglitz, M. Lability of DOC transported by Alaskan rivers to the Arctic Ocean.

908   *Geophysical Research Letters* **2008**, 35.

909   (40) Michaelson, G.; Ping, C.; Kling, G.; Hobbie, J. The character and bioactivity of

910   dissolved organic matter at thaw and in the spring runoff waters of the arctic tundra north

911   slope, Alaska. *Journal of Geophysical Research: Atmospheres (1984–2012)* **1998**, 103,

912   28939.

913   (41) Lipson, D. A.; Jha, M.; Raab, T. K.; Oechel, W. C. Reduction of iron (III) and humic

914   substances plays a major role in anaerobic respiration in an Arctic peat soil. *J. Geophys.*

915   *Res.* **2010**, 115, G00I06.

916   (42) Lipson, D. A.; Raab, T. K.; Goria, D.; Zlamal, J. The contribution of Fe(III) and

917   humic acid reduction to ecosystem respiration in drained thaw lake basins of the Arctic

918   Coastal Plain. *Global Biogeochemical Cycles* **2013**, 1.

919   (43) Merck, M. F.; Neilson, B. T.; Cory, R. M.; Kling, G. W. Variability of in-stream and

920   riparian storage in a beaded arctic stream. *Hydrol. Proc.* **2012**, 26, 2938.

921   (44) Page, S. E.; Arnold, W. A.; McNeill, K. Terephthalate as a probe for

922   photochemically generated hydroxyl radical. *J. Environ. Monit.* **2010**, 12, 1658.

923   (45) Cory, R. M.; Miller, M. P.; McKnight, D. M.; Guerard, J. J.; Miller, P. L. Effect of

924   instrument-specific response on the analysis of fulvic acid fluorescence spectra.

925   *Limnology and Oceanography: Methods* **2010**, 8, 67.

926 (46) Stookey, L. L. Ferrozine---a new spectrophotometric reagent for iron. *Anal. Chem.*

927 **1970**, 42, 779.

928 (47) Zeng, T.; Arnold, W. A. Pesticide photolysis in prairie potholes: Probing

929 photosensitized processes. *Environ. Sci. Technol.* **2013**.

930 (48) Razavi, B.; Ben Abdelmelek, S.; Song, W.; O'Shea, K. E.; Cooper, W. J.

931 Photochemical fate of atorvastatin (lipitor) in simulated natural waters. *Water Res.* **2011**,

932 45, 625.

933 (49) Santoke, H.; Song, W.; Cooper, W. J.; Peake, B. M. Advanced oxidation treatment

934 and photochemical fate of selected antidepressant pharmaceuticals in solutions of

935 Suwannee River humic acid. *Journal of hazardous materials* **2012**, 217, 382.

936 (50) Song, W.; Yan, S.; Cooper, W. J.; Dionysiou, D. D.; O'Shea, K. E. Hydroxyl Radical

937 Oxidation of Cylindrospermopsin (Cyanobacterial Toxin) and Its Role in the

938 Photochemical Transformation. *Environ. Sci. Technol.* **2012**, 46, 12608.

939 (51) Wang, L.; Xu, H.; Cooper, W. J.; Song, W. Photochemical fate of beta-blockers in

940 NOM enriched waters. *Science of the Total Environment* **2012**, 426, 289.

941 (52) Xu, H.; Cooper, W. J.; Jung, J.; Song, W. Photosensitized degradation of amoxicillin

942 in natural organic matter isolate solutions. *Water Res.* **2011**, 45, 632.

943 (53) Yang, W.; Ben Abdelmelek, S.; Zheng, Z.; An, T.; Zhang, D.; Song, W.

944 Photochemical transformation of terbutaline (pharmaceutical) in simulated natural waters:

945 Degradation kinetics and mechanisms. *Water Res.* **2013**, 47, 6558.

946 (54) Coelho, C.; Cavani, L.; Halle, A. t.; Guyot, G.; Ciavatta, C.; Richard, C. Rates of

947 production of hydroxyl radicals and singlet oxygen from irradiated compost.

948 *Chemosphere* **2011**, 85, 630.

949 (55) Luo, X.; Zheng, Z.; Greaves, J.; Cooper, W. J.; Song, W. Trimethoprim: Kinetic and

950 mechanistic considerations in photochemical environmental fate and AOP treatment.

951 *Water Res.* **2012**, 46, 1327.

952 (56) Nkhili, E.; Boguta, P.; Bejger, R.; Guyot, G.; Sokołowska, Z.; Richard, C.

953 Photosensitizing properties of water-extractable organic matter from soils. *Chemosphere*

954 **2013**.

955 (57) Page, S. E.; Sander, M.; Arnold, W. A.; McNeill, K. Hydroxyl radical formation

956 upon oxidation of reduced humic acids by oxygen in the dark. *Environ. Sci. Technol.*

957 **2012**, 46, 1590.

958 (58) Remucal, C. K.; McNeill, K. Photosensitized Amino Acid Degradation in the

959 Presence of Riboflavin and Its Derivatives. *Environ. Sci. Technol.* **2011**, 45, 5230.

960 (59) Fang, X.; Mark, G.; von Sonntag, C. OH Radical Formation by Ultrasound in

961 Aqueous Solutions Part I: The Chemistry Underlying the Terephthalate Dosimeter.

962 *Ultrason. Sonochem.* **1996**, 3, 57.

963 (60) Mark, G.; Tauber, A.; Laupert, R.; Schuchmann, H.-P.; Schulz, D.; Mues, A.; von

964 Sonntag, C. OH-Radical Formation by Ultrasound in Aqueous Solution - Part II:

965 Terephthalate and Fricke Dosimetry and the Influence of Various Conditions on the

966 Sonolytic Yield. *Ultrason. Sonochem.* **1998**, 5, 41.

967 (61) Saran, M.; Summer, K. H. Assaying for Hydroxyl Radicals: Hydroxylated

968 Terephthalate is a Superior Fluorescence Marker than Hydroxylated Benzoate. *Free*

969 *Radical Res.* **1999**, 31, 429

970 (62) Dulin, D.; Mill, T. Development and evaluation of sunlight actinometers. *Environ.*

971 *Sci. Technol.* **1982**, 16, 815.

972 (63) Vione, D.; Falletti, G.; Maurino, V.; Minero, C.; Pelizzetti, E.; Malandrino, M.;

973 Ajassa, R.; Olariu, R. I.; Arsene, C. Sources and Sinks of Hydroxyl Radicals upon

974 Irradiation of Natural Water Samples. *Environ. Sci. Technol.* **2006**, 40, 3775.

975 (64) Qian, J.; Mopper, K.; Kieber, D. J. Photochemical Production of the Hydroxyl

976 Radical in Antarctic Waters. *Deep Sea Res.* **2001**, 48, 741.

977 (65) Morris, D. P.; Zagarese, H.; Williamson, C. E.; Balseiro, E. G.; Hargreaves, B. R.;

978 Modenutti, B.; Moeller, R.; Queimalinos, C. The attenuation of solar UV radiation in

979 lakes and the role of dissolved organic carbon. *Limnol. Oceanogr.* **1995**, 40, 1381.

980 (66) Harrold, K. K.; Kling, G. W.; Papworth, B. N.; Neilson, B. T.; Cory, R. M. The role

981 of sunlight in the fate and export of DOM from a beaded arctic stream. *in preparation*.

982 (67) Grannas, A. M.; Martin, C. B.; Yu-Ping, C.; Platz, M. Hydroxyl Radical Production

983 from Irradiated Arctic Dissolved Organic Matter. *Biogeochem.* **2006**, 78, 51.

984 (68) Aeschbacher, M.; Graf, C.; Schwarzenbach, R. P.; Sander, M. Antioxidant properties

985 of humic substances. *Environ. Sci. Technol.* **2012**, 46, 4916.

986 (69) Ritchie, J. D.; Perdue, E. M. Proton-binding study of standard and reference fulvic

987 acids, humic acids, and natural organic matter. *Geochim. Cosmochim. Acta* **2003**, 67, 85.

988 (70) Thorn, K. A.; Folan, D. W.; MacCarthy, P. *Characterization of the International*

989 *Humic Substances Society standard and reference fulvic and humic acids by solution*

990 *state carbon-13 (13C) and hydrogen-1 (1H) nuclear magnetic resonance spectrometry*,

991 U.S. Geological Survey, 1989.

992 (71) McKnight, D. M.; Aiken, G. R. In *Aquatic humic substances*; Springer: 1998, p 9.

993 (72) Kujawinski, E. B.; Del Vecchio, R.; Blough, N. V.; Klein, G. C.; Marshall, A. G.

994 Probing molecular-level transformations of dissolved organic matter: insights on

995 photochemical degradation and protozoan modification of DOM from electrospray

996   ionization Fourier transform ion cyclotron resonance mass spectrometry. *Mar. Chem.*

997   **2004**, 92, 23.

998   (73) *Arctic LTER Synthesis Book*; Hobbie, J. E.; Kling, G. W., Eds.; Oxford University

999   Press, in press.

1000   (74) Allen, J. M.; Lucas, S.; Allen, S. K. Formation of hydroxyl radical (•OH) in

1001   illuminated surface waters contaminated with acidic mine drainage. *Environ. Toxicol.*

1002   *Chem.* **1996**, 15, 107.

1003   (75) Rosario-Ortiz, F. L.; Mezyk, S. P.; Doud, D. F. R.; Snyder, S. A. Quantitative

1004   Correlation of Absolute Hydroxyl Radical Rate Constants with Non-Isolated Effluent

1005   Organic Matter Bulk Properties in Water. *Environ. Sci. Technol.* **2008**, 42, 5924.

1006   (76) Westerhoff, P.; Aiken, G.; Amy, G.; Debroux, J. Relationships between the Structure

1007   of Natural Organic Matter and Its Reactivity towards Molecular Ozone and Hydroxyl

1008   Radicals. *Water Res.* **1999**, 33, 2265.

1009   (77) Westerhoff, P.; Mezyk, S. P.; Cooper, W. J.; Minakata, D. Electron Pulse Radiolysis

1010   Determination of Hydroxyl Radical Rate Constants with Suwannee River Fulvic Acid and

1011   Other Dissolved Organic Matter Isolates. *Environ. Sci. Technol.* **2007**, 41, 4640.

1012   (78) de Bruyn, W. J.; Clark, C. D.; Pagel, L.; Takehara, C. Photochemical Production of

1013   Formaldehyde, Acetaldehyde and Acetone from Chromophoric Dissolved Organic Matter

1014   in Coastal Waters. *J. Photochem. Photobiol., A* **2011**, 226, 16.

1015   (79) Vähätalo, A. V.; Salkinoja-Salonen, M.; Taalas, P.; Salonen, K. Spectrum of the

1016   quantum yield for photochemical mineralization of dissolved organic carbon in a humic

1017   lake. *Limnol. Oceanogr.* **2000**, 45, 664.

1018   (80) Latch, D. E.; McNeill, K. Microheterogeneity of Singlet Oxygen Distributions in

1019   Irradiated Humic Acid Solutions. *Science* **2006**, 311, 1743.

1020   (81) Lindsey, M. E.; Tarr, M. A. Inhibition of hydroxyl radical reaction with aromatics by

1021   dissolved natural organic matter. *Environ. Sci. Technol.* **2000**, 34, 444.

1022   (82) Grandbois, M.; Latch, D. E.; McNeill, K. Microheterogeneous concentrations of

1023   singlet oxygen in natural organic matter isolate solutions. *Environ. Sci. Technol.* **2008**,

1024   42, 9184.

1025   (83) Neilson, B. T., personal communication to Rose M. Cory, 2012.

1026